Chapter 6

Nanoplatform Based on Vertical Nanographene

Mineo Hiramatsu, Hiroki Kondo and Masaru Hori

Additional information is available at the end of the chapter

http://dx.doi.org/10.5772/61318

Abstract

Self-organized graphite sheet nanostructures composed of graphene have been studied intensively. Carbon nanowalls and related sheet nanostructures are layered graphenes with open boundaries. The sheets form a self-supported network of wall structures with thicknesses in the range from a few nanometers to a few tens of nanometers, and with a high aspect ratio. The large surface area and sharp edges of carbon nanowalls could prove useful for a number of different applications. Fabrication techniques of carbon nanowalls and possible applications using carbon nanowalls as nanoplatform in the area of electrochemistry and tissue engineering have been described. Radical injection technique was successfully applied to fabricate straight and large-size monolithic carbon nanosheet. The structure of carbon nanowalls was controlled by changing the total pressure and input power. In addition, the structure of carbon nanowalls was modified by O_2 plasma etching and H_2O_2 treatment. Using carbon nanowalls as platform would be the most promising and important application. Carbon nanowalls were used as electrode to detect several biomolecules. In addition, carbon nanowalls were oxidized by the surface treatment using atmospheric pressure plasma, and proteins such as bovine serum albumin were immobilized on these surface. Moreover, carbon nanowalls were used as scaffold for cell culturing. The dependence of the cell culturing rates and morphological changes of HeLa cells on carbon nanowall scaffolds with different densities and wettability were systematically investigated. Nanoplatform based on vertical nanographene offers great promise for providing a new class of nanostructured electrodes for electrochemical sensing, biosensing and energy conversion applications.

Keywords: carbon nanowalls, vertical nanographene, nanoplatform, electrochemistry, biosensing

1. Introduction

It is well known that sp^2 carbon can lead to various kinds of layered structures. Among these structures, graphene (monolayer and few layers) is an actual two-dimensional material with

the large anisotropy between the in-plane and out-of-plane directions. Planar graphene films with respect to the substrate have been synthesized by thermal decomposition of carbon-terminated silicon carbide and chemical vapor deposition (CVD) on metals such as nickel (Ni) and copper (Cu) substrates [1-3]. On the other hand, plasma-enhanced CVD (PECVD) is among the early methods to synthesize vertically standing carbon sheet structures [4-17]. These structures are called as carbon nanowalls (CNWs), carbon nanoflakes, and carbon nanosheets. CNWs and related nanocarbon structures consist of nanographene sheets standing vertically on a substrate. Figure 1 shows a schematic illustration of CNWs, where few-layer graphenes composed of nanographite domains form a self-supported network of wall structures. The mazelike architecture of CNWs with large-surface-area graphene planes and a high density of graphene edges would be useful as platform for electrochemical applications as well as tissue engineering such as scaffold for cell culturing [18-25].

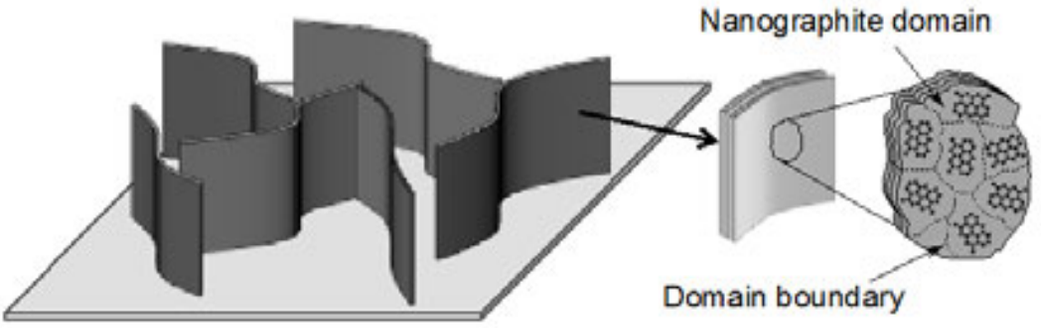

Figure 1. Schematic illustration of CNWs.

CNWs and related sheet nanostructures have been synthesized using several PECVD techniques, which are similar to those utilized for growing carbon nanotubes (CNTs) and diamond thin films. For the growth of CNWs, typically, a mixture of methane (CH_4) and hydrogen (H_2) is employed as source gases. A certain amount of hydrogen (H) atoms are required for growing CNWs. In general, microwave plasma and inductively coupled plasma (ICP) have been used for the growth of CNWs. These are high-density plasmas and are suitable for decomposing H_2 molecules efficiently. Or more specifically, radio frequency (rf) capacitively coupled plasma (CCP) with H radical injection and very high frequency (VHF) plasma with H radical injection have been applied to synthesize of CNWs. Pressures are ranging from 1 Pa to atmospheric pressure. Preparation of metal catalysts such as iron (Fe) and cobalt (Co) on the substrate is essential for the growth of CNTs. Unlike the CNT growth, CNWs do not require such catalysts for their nucleation. CNW growth has been conducted on several substrates including Si, SiO_2, and Al_2O_3 without the use of catalysts at substrate temperatures of 500-700°C [5]. In view of the practical use of CNWs for device applications such as biosensors or electrochemical sensors in micrototal analysis system, further investigations should be performed to enable control of structures and surface properties of CNWs.

In this chapter, fabrication techniques of CNWs and possible applications using CNWs as nanoplatform in the area of electrochemistry and tissue engineering are described. In the

http://dx.doi.org/10.5772/61318

beginning, characterizations of CNWs are outlined. Then synthesis method for CNWs using VHF CCP with H radical injection is presented. Radical injection technique was successfully applied to fabricate straight and large-size monolithic carbon nanosheet. The VHF CCP with H radical injection was developed with the aim of achieving large-area growth of CNWs with a reasonable growth rate. The structure of CNWs was controlled by changing the total pressure and VHF power. In addition, the structure of CNWs was modified by O_2 plasma etching and hydrogen peroxide (H_2O_2) treatment.

In the latter half of this chapter, the electrochemical application of CNWs is described. Biosensing with CNWs is a promising application. Dopamine, ascorbic acid, and uric acid are compounds of great biomedical interest, which all are essential biomolecules in our body fluids. CNWs were used as electrode to detect these biomolecules. In addition, CNWs were oxidized by the surface treatment using atmospheric pressure plasma, and proteins such as bovine serum albumin were immobilized on these surface. Electrochemical properties of surface-decorated electrodes were investigated. Moreover, CNWs were used as scaffold for cell culturing. The dependence of the cell-culturing rates and morphological changes of HeLa cells on CNW scaffolds with different densities and wettability were systematically investigated.

2. Brief description of carbon nanowalls

CNWs are mazelike architecture consisting of few-layer graphenes standing vertically on a substrate, as was illustrated in Figure 1. The CNW sheet itself is composed of nanodomains of a few tens of nanometers in size. Scanning electron microscopy (SEM) images of CNWs with different morphology are shown in Figures 2(a) -2(d). The morphology of CNWs depends on the synthesis conditions, including pressure, substrate temperature, source gas mixtures, and the type of plasma used for the synthesis. Typical mazelike architecture (Figure 2(a)), isolated vertical nanosheets (Figure 2(b)), and highly branched type (Figure 2(c)) have been fabricated. Moreover, straight and aligned CNWs with regular spacing (Figure 2(d)) was obtained on the substrate set perpendicular to the electrode plate in the case of growth using rf CCP with H radical injection [9].

Figures 3(a) and 3(b) show typical transmission electron microscopy (TEM) images of CNW with a micrometer-high planar nanosheet structure, which was synthesized using electron beam excited plasma-enhanced CVD [12]. Despite the relatively smooth surface, each sheet in CNWs is actually composed of nanographite domains of a few tens of nanometers distinguished by domain boundaries as shown in Figure 3(a). Graphene layers are clearly observed in the high-resolution TEM image of the CNW shown in Figure 3(b). The spacing between neighboring graphene layers was approximately 0.34 nm.

Figure 4 shows a typical Raman spectrum of CNW film formed on Si substrate, which was measured at room temperature using a 514.5-nm line of an argon laser. Typical Raman spectrum for the CNWs has two strong peaks at 1590 cm^{-1} (G band), indicating the formation of graphitized structure and at 1350 cm^{-1} (D band) corresponding to the disorder-induced

Figures 3(a) and 3(b) show typical transmission electron microscopy (TEM) images of CNW with a micrometer-high planar nanosheet structure, which was synthesized using electron beam excited plasma-enhanced CVD [12]. Despite the relatively smooth surface, each sheet in CNWs is actually composed of nanographite domains of a few tens of nanometers distinguished by domain boundaries as shown in Figure 3(a). Graphene layers are clearly observed in the high-resolution TEM image of the CNW shown in Figure 3(b). The spacing between neighboring graphene layers was approximately 0.34 nm.

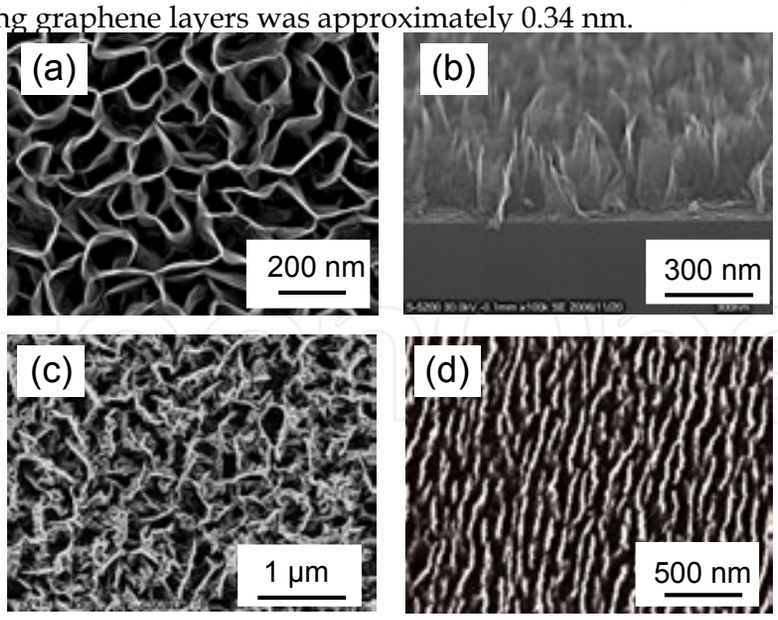

Figure 2. SEM images of CNWs with different morphologies.

Figure 2. SEM images of CNWs with different morphologies.

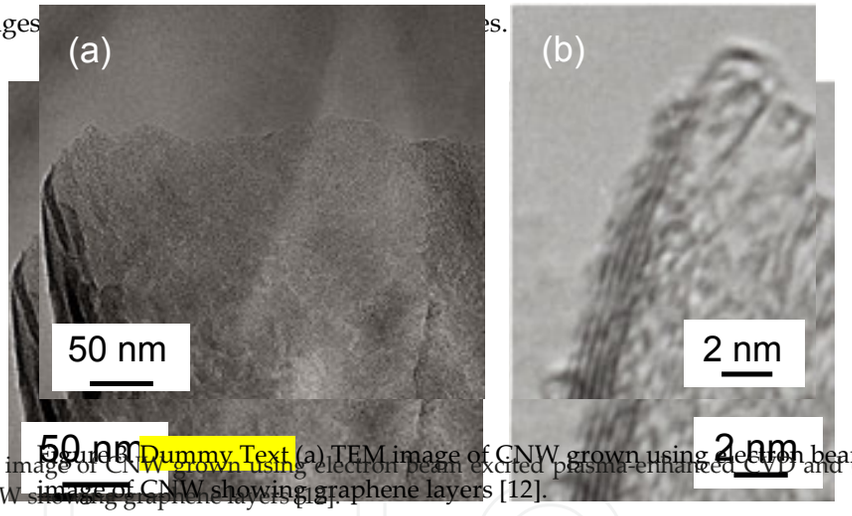

Figure 3. (a) TEM image of CNW grown using electron beam excited plasma-enhanced CVD and (b) high-resolution TEM image of CNW showing graphene layers [12].

Figure 3. (a) TEM image of CNW grown using electron beam excited plasma-enhanced CVD and (b) high-resolution TEM image of CNW showing graphene layers [12].

Figure 4 shows a typical Raman spectrum of CNW film formed on Si substrate, which was measured at room temperature using a 514.5-nm line of an argon laser. Typical Raman spectrum for the CNWs has two strong peaks at 1575 cm^{-1} (G band) corresponding to graphitized structure and at 1350 cm^{-1} (D band) corresponding to the presence of graphene edges and small graphite domains. It is noted that the G band peak is accompanied by a shoulder peak at 1620 cm^{-1}. This shoulder peak is often designated as D' band and associated with finite-size graphite crystals and graphene edges [8,11,13]. The strong 2D band peak at 2690 cm^{-1} is used to confirm the presence of few-layer graphene. It originates from a double resonance process that links phonons to the electronic band structure [28,29].

Figure 4 shows a typical Raman spectrum of CNW film formed on Si substrate, which was measured at room temperature using a 514.5-nm line of an argon laser. Typical Raman spectrum for the CNWs has two strong peaks at 1575 cm^{-1} (G band) corresponding to graphitized structure and at 1350 cm^{-1} (D band) corresponding to the presence of graphene edges and small graphite domains. It is noted that the G band peak is accompanied by a shoulder peak at 1620 cm^{-1}. This shoulder peak is often designated as D' band and associated with finite-size graphite crystals and graphene edges [8,11,13]. The strong 2D band peak at 2690 cm^{-1} is used to confirm the presence of few-layer graphene. It originates from a double resonance process that links phonons to the electronic band structure [28,29].

Carbon materials such as grassy carbon and conductive doped diamond have been widely used in both analytical and industrial electrochemistry due to their low cost, wide potential window, relatively low background current, and activity for a variety of redox

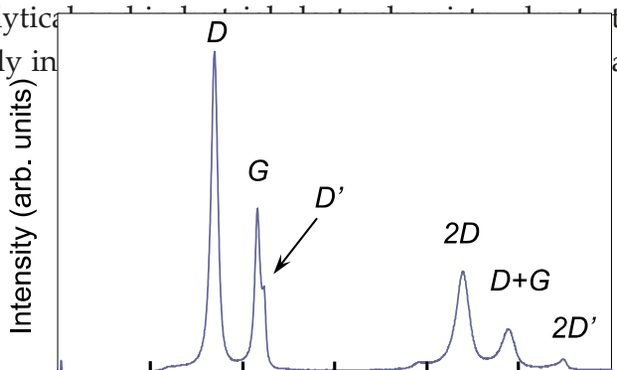

band peak suggests a more nanocrystalline structure, and the presence of graphene edges is noted that the G band peak is accompanied by a shoulder peak at 1620 cm^{-1}. This should D′ band and associated with finite-size graphite crystals and graphene edges [26,27]. The s and D′ band peak are prevalent features of CNWs [8,11,13]. The 2D band peak at 2690 cm^{-1} i of few-layer graphene. It originates from a double resonance process that links phonons to [28,29].

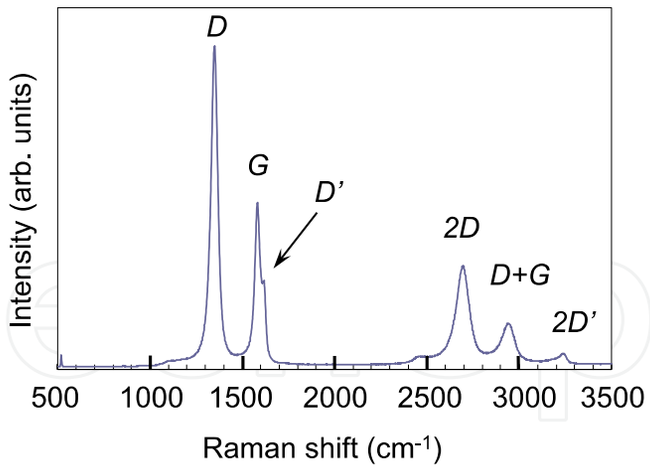

Figure 4. Typical Raman spectrum of CNWs.

Figure 4. Typical Raman spectrum of CNWs.

reactions. For the electrochemical applications, these carbon-based electrodes are often decorated with catalyst nanoparticles such as platinum (Pt). As was illustrated in Figure 1, CNW film has many graphene edges, and the CNW sheet itself is composed of nanographite domains of a few tens of nanometers in size. These graphene edges and domain boundaries are chemically reactive and are modified easily with several types of surface termination, e.g. C-NH_2, C-OH, and C-COOH. Furthermore, Pt nanoparticles were preferably deposited on the defects such as grain boundaries on the surface of graphite [24]. Therefore, the structure of CNWs can be suitable for the platform of the electrochemical and biosensing applications. This kind of vertical-nanographene-based electrochemical platform with the high surface area and electrocatalytic activity offers great promise for electrochemical sensing and biosensing, fuel cells and energy-conversion electrodes for electrochemical sensing and biosensing, fuel cells and energy-conversion applications.

Carbon materials such as grassy carbon and conductive doped diamond have been widel industrial electrochemistry due to their low cost, wide potential window, relatively electrocatalytic activity for a variety of redox reactions. For the electrochemical app electrodes are often decorated with catalyst nanoparticles such as platinum (Pt). As was illu has many graphene edges, and the CNW sheet itself is composed of nanographite domains size. These graphene edges and domain boundaries are chemically reactive and are modifi surface termination, e.g., C-NH_2, C-OH, and C-COOH. Furthermore, Pt nanoparticles wer defects such as grain boundaries on the surface of graphite [24]. Therefore, the structure of platform of the electrochemical and biosensing applications. This kind of vertical-nanogr platform with the high surface area and electrocatalytic activity offers great promis ity offers great promise for electrochemical sensing and biosensing, fuel cells and energy

The morphology and electrical properties of CNW film depend on the synthesis conditions, including source gases, pressure, process temperature, and the type of plasma used for the growth of CNWs. We can, therefore, expect a wide variety of applications based on their structure or electrical properties. For the electron emitters, CNWs with a vertically thin edge, moderate spacing, and excellent height uniformity are required. For the membrane filter using honeycomb structure of CNWs, the spacing between adjacent nanowalls should be controlled. Moreover, CNWs should be detached from the substrate to obtain freestanding membrane, and the CNW membrane should be attached to the different materials. On the other hand, less aligned, dense CNW film with large surface area can be used as gas storage application, while vertical alignment and crystallinity of CNWs can be less crucial.

The morphology and electrical properties of CNW film depend on the synthesis condi pressure, process temperature, and the type of plasma used for the growth of CNWs. We applications based on their structure or electrical properties. For the electron emitters, CNW moderate spacing, and excellent height uniformity are required. For the membrane filter CNWs, the spacing between adjacent nanowalls should be controlled. Moreover, CNWs substrate to obtain freestanding membrane, and the CNW membrane should be attached to other hand, less aligned, dense CNW film with large surface area can be used as gas stor alignment and crystallinity of CNWs can be less crucial.

In view of the practical applications using CNWs, desirable structures and electrical and chemical properties of CNWs depend on the area of their applications. Therefore, structures, electrical properties, surface chemical properties of CNWs and related sheet nanostructures should be controlled according to their applications. Although the nucleation mechanism of CNWs is still unclear, ion bombardment on the substrate would have some effect on the

In view of the practical applications using CNWs, desirable structures and electrical and depend on the area of their applications. Therefore, structures, electrical properties, surface and related sheet nanostructures should be controlled according to their applicatio mechanism of CNWs is still unclear, ion bombardment on the substrate would have so nanographene at the very early growth stage [30]. The growth of CNWs was enhanced substrates such as Ni and iron (Fe) [4]. The spacing between adjacent nanowalls and thic affected by the density ratio of C_xH_y radicals to H atoms [31]. The addition of Ar into the secondary nucleation at the wall surface, resulting in the formation of highly branched volume ratio as shown in Figure 2(c). On one hand, branching could be suppressed and stra carbon nanosheet could be obtained by the addition of oxygen into the source gas [32]. I CNWs for device applications such as biosensors or electrochemical sensors in the form

application, while vertical alignment and crystallinity of CNWs can be less crucial.

In view of the practical applications using CNWs, desirable structures and electrical and chemical properties of CNWs depend on the area of their applications. Therefore, structures, electrical properties, surface chemical properties of CNWs, and related sheet nanostructures should be controlled according to their applications. Although the nucleation mechanism of CNWs is still unclear, ion bombardment on the substrate would have some effect on the nucleation of nanographene at the very early growth stage [30]. The growth of CNWs was enhanced occasionally by using metal substrates such as Ni and iron (Fe) [4]. The spacing between adjacent nanowalls and thickness of nanowalls would be affected by the density ratio of C_xH_y radicals to H atoms [31]. The addition of Ar into the source gas would induce the secondary nucleation at the wall surface, resulting in the formation of highly branched CNWs with high surface to volume ratio as shown in Figure 2(c). On one hand, branching could be suppressed and straight and large-size monolithic carbon nanosheet could be obtained by the addition of oxygen into the source gas [32]. In view of the practical use of CNWs for device applications such as biosensors or electrochemical sensors in the form of micrototal analysis system, postprocesses such as integration techniques, including etching and coating of CNWs and surface functionalization should be established. Figure 5 shows schematic illustration of CNW structures that should be controlled in the nucleation and growth stages and modified by the postprocesses, including etching and surface functionalization. Hereafter, we describe the recent development of CNW fabrication with emphasis on the structure control for realizing carbon nanoplatform working in the area of electrochemical and bio applications.

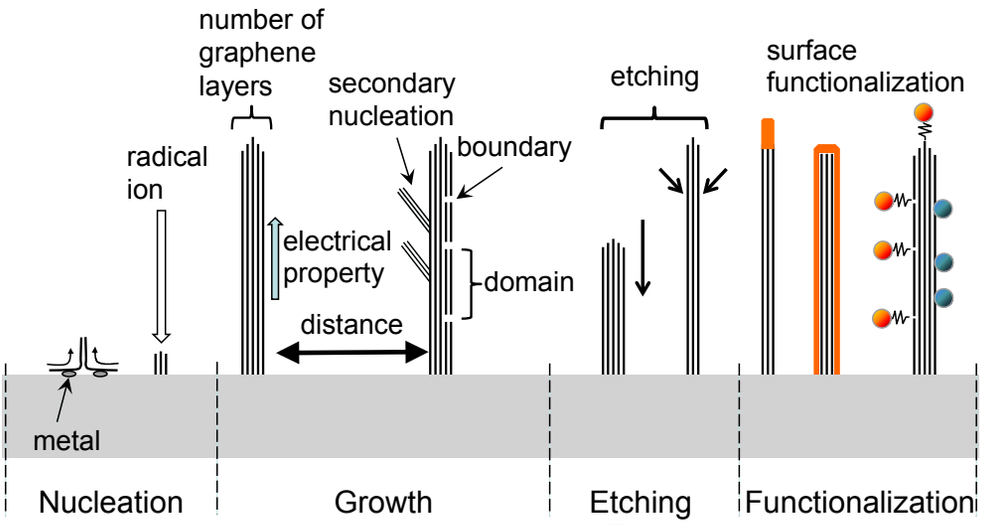

Figure 5. Schematic illustration of structures of CNWs to be controlled in the nucleation and growth stages and modified by the postprocesses, including etching and surface functionalization.

3. Fabrication of carbon nanowalls using Radical Injection Plasma Enhance Chemical Vapor Deposition (RI-PECVD)

3.1. Growth of carbon nanowalls from fluorocarbon/hydrogen mixture

In the case of PECVD with hydrocarbon/hydrogen system, for example, both CH_3 radical and H atoms are thought to play important roles in the formation of several carbon structures. The parallel-plate CCP might be useful to produce plenty of hydrocarbon radicals such as CH_3

http://dx.doi.org/10.5772/61318

radicals effectively [33] and also useful for the large-area deposition of the film. However, the CCP itself is not suitable for the growth of diamond and nanodiamond films because of the shortage of H atoms [34]. In contrast, high-density plasmas such as microwave plasma and ICP are suitable for dissociating H_2 molecules efficiently.

Proof Corrections Form

1. Final Chapter Title:Nanoplatform Based on Vertical Nanographene

2. Author details

Scientific Title: PhD.
Full Name:MinoHiramatsu
Affiliation:Meijo University
Position: Professor

Page No.	Line No.	Delete	Replace with
1	17	O2	O_2
1	18	H2O2	H_2O_2
2	Fig. 1		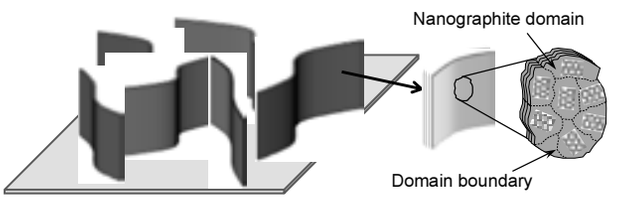
3	29	3(b)show	3(b)show
5	25	CNWs, and	CNWs and
7	Fig. 6		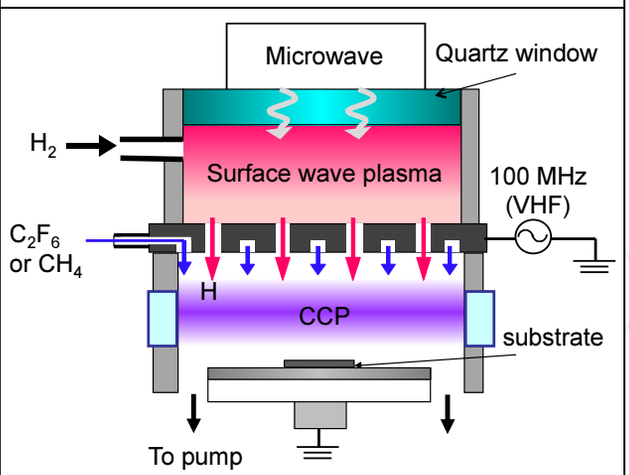
9	20	this layer was composed of	this layer composed of
10	25	Figures 10(a) -10(d)show	Figures 10(a)-10(d)show
14	10	14(b)show	14(b)show
15	5	16(f)was	16(f)was

Figure 6. Schematic of VHF plasma assisted by H_2 microwave surface wave plasma [14,35].

Figure 7(a) shows the H and C atom densities in the VHF plasma of RI-PECVD employing C_2F_6/H_2 mixture, together with the height variation of CNW films. The measurement of atom densities was conducted using the vacuum ultraviolet absorption spectroscopy (VUVAS) system as a function of the total pressure during the CNW growth at microwave and VHF

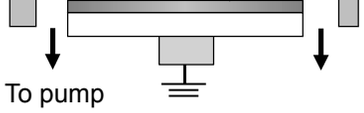

Figure 6. Schematic of VHF plasma assisted by H_2 microwave surface wave plasma [14,35].

Figure 7(a) shows the H and C atom densities in the VHF plasma of RI-PECVD employing C_2F_6/H_2 m
powers of 250 and 270 W, and C_2F_6 and H_2 flow rates of 50 and 100 sccm, respectively [35]. As
the total pressure increased in the range from 0.1 to 0.6 torr (13.3 to 80 Pa), the H atom density
increased drastically from 10^{12} to 10^{14} cm^{-3}, while the C atom density was almost constant at 5
× 10^{12} cm^{-3}, as shown in Figure 7(a). In contrast, the height of the CNW films decreased with
an increase in the total pressure. SEM images of CNWs grown at different total pressures are
shown in Figures 7(b)–7(d) [35]. CNW film with narrow interspaces was obtained at a low
total pressure of 0.1 torr (13.3 Pa), while CNW film with wider interspaces of 30-40 nm was
grown at a high pressure of 0.6 torr (80 Pa). As the H/C atom density ratio increased, the growth
rate of the CNWs increased, the average diameter of the CNWs decreased, and the average interspaces betwe
wider.

VHF powers of 250 and 270 W, and C_2F_6 and H_2 flow rates of 50 and 100 sccm, respectively [35]. A
increased in the range from 0.1 to 0.6 torr (13.3 to 80 Pa), the H atom density increased drastically fr
while the C atom density was almost constant at 5 × 10^{12} cm^{-3}, as shown in Figure 7(a). In contrast, th
films decreased with an increase in the total pressure. SEM images of CNWs grown at different total
in Figures 7(b)–7(d) [35]. CNW film with narrow interspaces was obtained at a low total pressure
while CNW film with wider interspaces of 30-40 nm was grown at a high pressure of 0.6 torr (80 P
density ratio increased, the growth rate of the CNWs increased, the average diameter of the CNWs decreased, and the average interspaces betwe
wider.

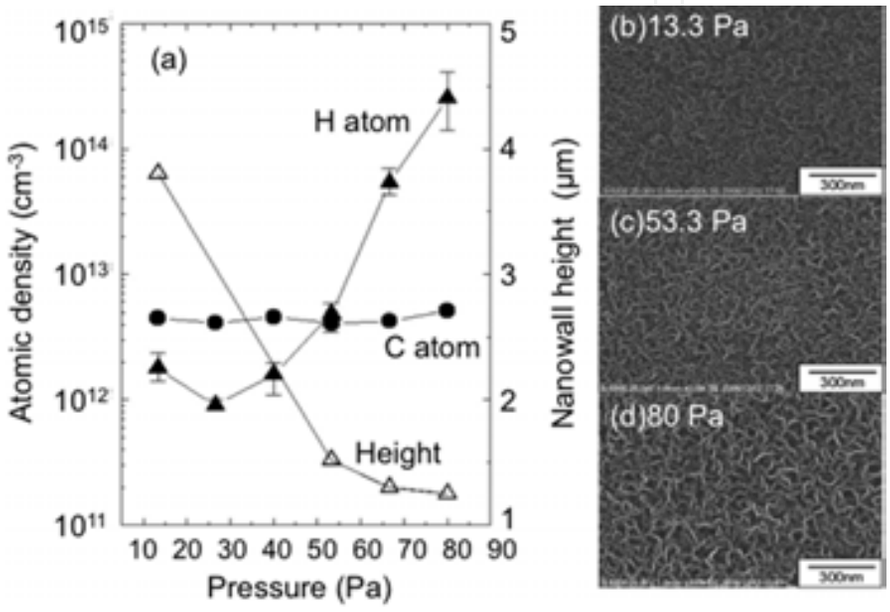

Figure 7. (a) H and C atom densities in VHF plasma employing C_2F_6/H_2 mixtures, together with the height variation of CNW films, as a function of total pressure during the CNW formation at a microwave power of 250 W and a VHF power of 270 W, (b-d) SEM images of CNWs grown at pressures of 0.1, 0.4, and 0.6 torr (13.3, 53.3 and 80 Pa), respectively [35].

Figure 7. Dummy Text (a) H and C atom densities in VHF plasma employing C_2F_6/H_2 mixtures, together with the
CNW films, as a function of total pressure during the CNW formation at a microwave power of 250 W and a VHF
SEM images of CNWs grown at pressures of 0.1, 0.4, and 0.6 torr (13.3, 53.3 and 80 Pa), respectively [35].

In addition, O_2 and N_2 gases were introduced into the VHF-CCP region. The crystallinity of
vertically standing CNWs is improved by introducing O_2 into the plasma used for CNW
growth [32], while N addition is expected to control the electrical properties of the CNWs [35].
Figure 8(a) shows the cross-sectional SEM image of the typical CNW film grown on a Si
substrate, and the inset shows the top view SEM image of the same CNW film. CNW growth
was conducted on a Si substrate using a C_2F_6/H_2 mixture, resulting in the formation of slightly
branching carbon sheets standing almost vertically on the substrate, as shown in Figure 8(a).
The thickness of CNW film grown for 30 min was approximately 1 μm. Figure 8(b) shows TEM
image of CNWs grown using C_2F_6/H_2, where randomly oriented, small overlapping multilay-
ered graphene domains were observed. The inset shows magnified image of the area enclosed
by square, where a bent multilayered graphene structure with a thickness of approximately 9
nm was observed. In contrast, Figure 8(c) shows a cross-sectional SEM image of the CNW film
grown for 40 min using C_2F_6/H_2 with O_2 addition, and the inset shows the top view SEM image

In addition, O_2 and N_2 gases were introduced into the VHF-CCP region. The crystallinity of vertical
improved by introducing O_2 into the plasma used for CNW growth [32], while N addition is exp
electrical properties of the CNWs [35]. Figure 8(a) shows the cross-sectional SEM image of the typical
a Si substrate, and the inset shows the top view SEM image of the same CNW film. CNW growth w
Figure 8(a) shows the cross-sectional SEM image of the typical CNW film grown on a Si
substrate using a C_2F_6/H_2 mixture, resulting in the formation of slightly branching carbon she
vertically on the substrate, as shown in Figure 8(a). The thickness of CNW film grown for 30 min w
μm. Figure 8(b) shows TEM image of CNWs grown using C_2F_6/H_2, where randomly oriented
multilayered graphene domains were observed. The inset shows magnified image of the area enclose
bent multilayered graphene structure with a thickness of approximately 9 nm was observed. In

electrical properties of the CNWs [35]. Figure 8(a) shows the cross-sectional SEM image of the a Si substrate, and the inset shows the top view SEM image of the same CNW film. CNW gr substrate using a C_2F_6/H_2 mixture, resulting in the formation of slightly branching car vertically on the substrate, as shown in Figure 8(a). The thickness of CNW film grown for μm. Figure 8(b) shows TEM image of CNWs grown using C_2F_6/H_2, where randomly multilayered graphene domains were observed. The inset shows magnified image of the area

of the same CNW film. CNW films grown with O_2 had larger plane sheets with wider bent multilayered graphene structure with a thickness of approximately 7 nm was obser interspaces than those grown without O_2. By the addition of O_2, a film grown for 40 min using C_2F_6/H_2 wit source gas mixture shows the top view SEM image of the same CNW film. CNW films grown with O_2 had lar Figure 8(c). However, as a result of O_2 addition, the growth rate was reduced by approximately 33%. Figure 8(d) shows TEM image of CNWs grown with additional O_2, together with magnified image of square area as an inset. Monolithic self-sustaining graphene sheets larger than 200 nm in size were clearly observed in the CNWs grown with O_2. A highly orientated, smooth multilayered graphene structure was clearly observed in the inset of Figure 8(d) [32].

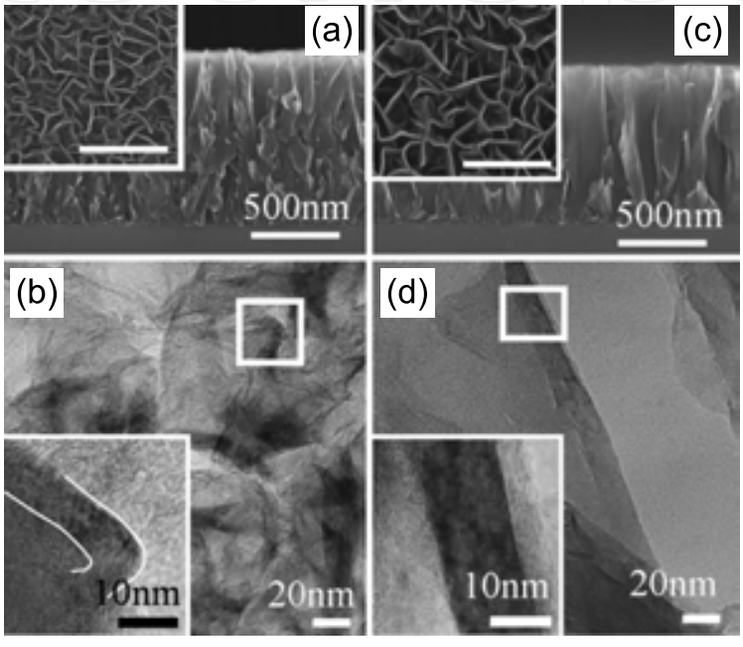

Figure 8. (a) Cross-sectional SEM image of CNW film grown on a Si substrate for 30 min using C_2F_6/H_2, together with SEM top view image of identical CNW film as an inset. (b) TEM image of bent CNWs grown using C_2F_6/H_2, together with magnified image of square area as an inset. (c) Cross-sectional SEM image of CNW film grown for 40 min using C_2F_6/H_2 with additional O_2 gas, together with SEM top view image of identical CNW film as an inset. (d) TEM image of straight CNWs grown with additional O_2, together with magnified image of square area as an inset [32].

Here, the morphology and structure of deposits formed using C_2F_6/H_2 in the early growth stage were investigated in detail. Figures 9(a)-9(d) show tilted SEM images of the deposits formed during the nucleation of CNW growth. At the very early stage of nucleation, as shown in Figure 9(a), nanoislands were formed on the Si substrate in 30 s. The density of nanoislands (number of nanoislands per area) increased with growth period. In 1 min, most of the surface of Si was covered with nanoislands (Figure 9(b)). The thickness of this layer composed of nanoislands was approximately 10 nm. At this moment, some nanoflakes have started to form at the aggregations of nanoislands forming the first layer. Subsequently, randomly oriented nanoflakes were formed on the first layer (Figure 9(c)). In 3 min, these sheet structures grow preferentially in a vertical direction to form vertical CNWs, while the number density of these nanoflakes was less than that observed at 2 min (Figure 9(d)). Figure 9(e) shows a cross-sectional TEM image of CNWs grown for 30 min, indicating that the interfacial layer exists

between the CNWs and the Si surface. The thickness of the interface layer is approximately 10 nm, which is identical to the thickness of the first layer formed during the nucleation stage. Similar interface layer was also observed in the CNW films grown on Si and SiO_2 substrates using inductively coupled plasma (ICP) with $CH_4/H_2/Ar$ mixtures [13].

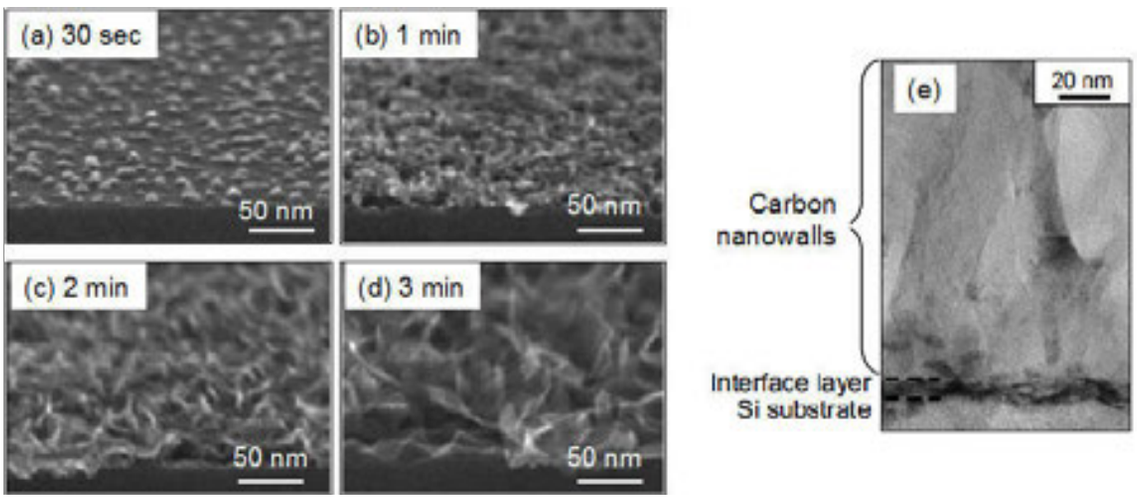

Figure 9. SEM images of the deposits formed on a Si substrate using a C_2F_6/H_2 system for (a) 30 s, (b) 1 min, (c) 2 min, and (d) 3 min. (e) Cross-sectional TEM image of CNWs and an interface layer synthesized for 30 min [14].

So far, several papers have been published on the observation of CNW growth in the early growth stage and the nucleation mechanism for the formation of vertical layered-graphenes on Si and SiO_2 substrates using various CVD methods [5,7,8,13-17,30]. It is common in previous studies that there is an induction period of 1-5 min for the nucleation of vertical nanographene. In addition, there exists an interface layer between the vertical nanographenes and substrate surface. Raman spectra were recorded for the deposits in the initial growth stages. D- and G-bands were not observed in the Raman spectra of nanoislands formed on the substrate for 1 min or less despite the fact that carbon was detected in these samples by X-ray photoelectron spectroscopy (XPS) analysis [14]. The nanoislands and the interface layer underlying two-dimensional nanographene are considered to be amorphous carbon. In most cases using several PECVD methods, the interface layer under the CNWs is considered to be an amorphous carbon [5,7,15,17,30,37]. Due to the existence of amorphous carbon interface layer, it is possible to grow CNWs and similar structures on a variety of substrates without catalyst. In contrast, Zhu et al. suggested that graphenes parallel to the substrate surface would grow at first. In their model, at the grain boundaries of these horizontal few-layer graphenes, spreading edge of the top layers of few-layer graphenes would curl upward, resulting in the vertical orientation of these sheets [8].

Figures 10(a)-10(d) show tilted SEM images of the deposits on the Si surface during the nucleation of CNW growth with O_2 addition. At 30 s, no deposits were observed on the surface [Figure 10(a)]. In 1 min, nanoislands were formed on the Si substrate [Figure 10(b)]. It took longer time to nucleate nanoislands in the case of the growth with O_2 gas addition, compared with the case without O_2 shown in Figure 9(a). In 2 min, some small two-dimensional nano-

http://dx.doi.org/10.5772/61318

flakes have started to grow at isolated nanoislands, while the fractional surface coverage was low, as shown in Figure 10(c). A distinct interface layer was not formed. As shown in Figure 10(d), isolated wall structures had grown in 3 min, while the number density of start-up CNWs was lower than that without O_2,

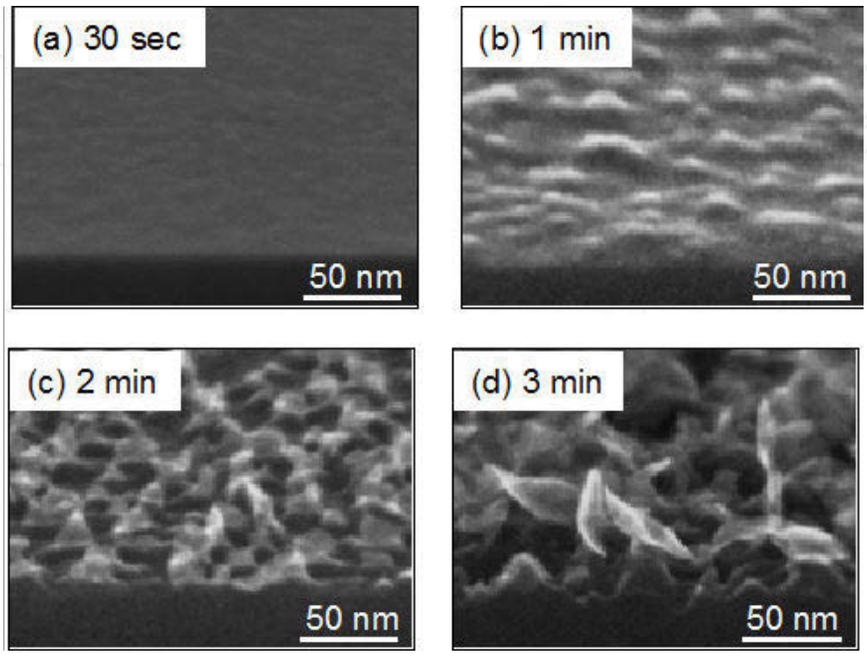

Figure 10. SEM images of the deposits formed on Si substrate using C_2F_6/H_2 with O_2 addition for (a) 30 s, (b) 1 min, (c) 2 min, and (d) 3 min [14].

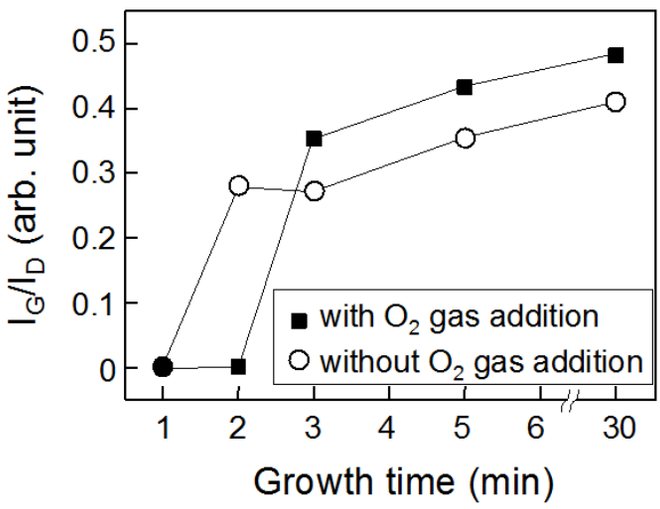

Figure 11. Temporal behaviors of I_G/I_D ratios of CNWs formed with and without O_2 gas addition [14].

Raman spectra were recorded for the deposits formed without and with O_2 addition in the initial growth stages. The intensity ratios of the G-band (I_G) to the D-band (I_D) of the deposits

formed with and without O_2 gas addition as functions of growth period are shown in Figure 11. In the case of the CNW growth without O_2 addition, distinct G-band peak was observed in 2 min, and the I_G/I_D ratio increased gradually with increasing growth period, indicating that vertical nanographene formation started after the 2-min growth. In the case of the CNW growth with O_2 addition, on the other hand, distinct G-band peak was observed at 3 min, indicating that vertical nanographene formation started after 3 min. Moreover, the I_G/I_D ratio was higher than that for the CNWs synthesized without O_2, revealing that the O_2 gas addition is effective for obtaining highly graphitized CNWs.

In the process without O_2 gas addition, amorphous nanoislands were formed on the Si substrate, and the Si surface was completely covered with these nanoislands in the initial stage, resulting in the formation of a 10-nm-thick amorphous carbon interface layer. Vertical nanographene started to grow at nuclei on the surface of the interface layer. On the other hand, distinct interface layer was not formed in the process with O_2 gas addition, and vertical nanographenes were formed on isolated nanoislands. O_2 gas addition to C_2F_6/H_2 is effective in suppressing the formation of carbon nanoislands and thereby in controlling CNW nucleation.

3.2. Growth of carbon nanowalls from methane/hydrogen mixture

As is obvious, CNWs can also be fabricated employing the CH_4/H_2 mixture using RI-PECVD. In terms of controlling the wall density (or interspaces between adjacent nanowalls), total pressure and VHF power were changed. In these experiments, the heights of the CNWs were adjusted to 800 ± 50 nm, by varying the growth period. For all growth conditions, the films were uniform and exhibited a similar morphology. The thickness of individual CNWs in the films was approximately 10 nm. To consider what chemical species would affect the determination of wall density in these experiments, a plasma diagnosis was carried out using optical emission spectroscopy (OES). By introducing Ar gas into plasma region with a flow rate of 3 sccm, the actinometric measurements were carried out. Here, for determining the relative densities of H atoms and CH radicals, the emission intensity ratios ([CH]/[Ar] and [Hα]/[Ar]) were monitored by detecting the spectral lines associated with Hα 656.1 nm (excitation threshold energy, E = 12.1 eV), CH 431.2 nm (E = 14.6 eV), and Ar 751.4 nm (E = 13.27 eV).

Figure 12 shows top view and cross-sectional SEM images of CNWs grown on SiO_2 substrates at total pressures of (a) 1 Pa, (b) 3 Pa, and (c) 5 Pa under a constant VHF power of 300 W. As the total pressure increased, the wall density decreased or interspaces between adjacent nanowalls increased. Figure 12(d) shows the intensities of the CH and Hα emissions relative to Ar as a function of total pressure at a constant VHF power of 300 W. As the total pressure increased, [CH]/[Ar] decreased and [H]/[Ar] increased. Figure 13 shows top view and cross-sectional SEM images of CNWs grown on SiO_2 substrates at VHF powers of (a) 200 W, (b) 300 W, and (c) 400 W under a constant total pressure of 1 Pa. As the VHF power increased, the wall density increased or interspaces between adjacent nanowalls decreased. As shown in Figure 13(d), [CH]/[Ar] increased and [H]/[Ar] decreased with the increase of VHF power. It was found from the results shown in Figures 12 and 13 that the wall density could be controlled using the total pressure and the VHF power. The above results suggest that H and CH radicals are the important chemical species and the density ratio [CH]/[H] can be useful and simple

http://dx.doi.org/10.5772/61318

index for controlling the wall density. Obviously, the OES provides information about only radicals of which optical emission transitions are permitted by selection rules. Other important carbon-containing species, including CH_3, CH_2, and C_2H_2 should be measured by other diagnostics such as absorption spectroscopy and mass spectrometry for further investigation on the growth mechanism.

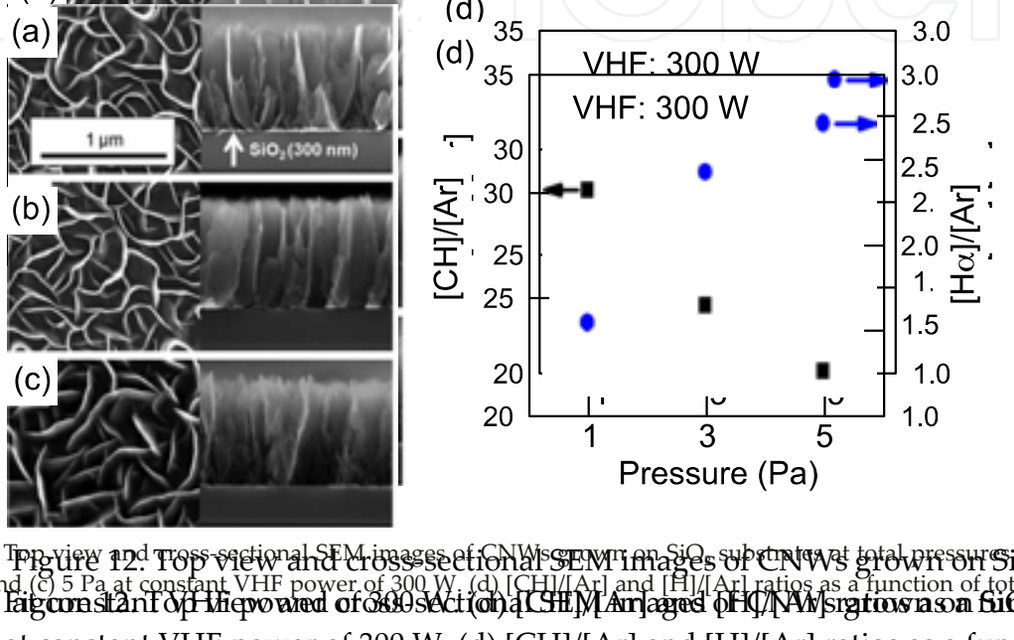

Figure 12. Top view and cross-sectional SEM images of CNWs grown on SiO_2 substrates at total pressures of (a) 1 Pa, (b) 3 Pa, and (c) 5 Pa at constant VHF power of 300 W. (d) [CH]/[Ar] and [H]/[Ar] ratios as a function of total pressure [31].

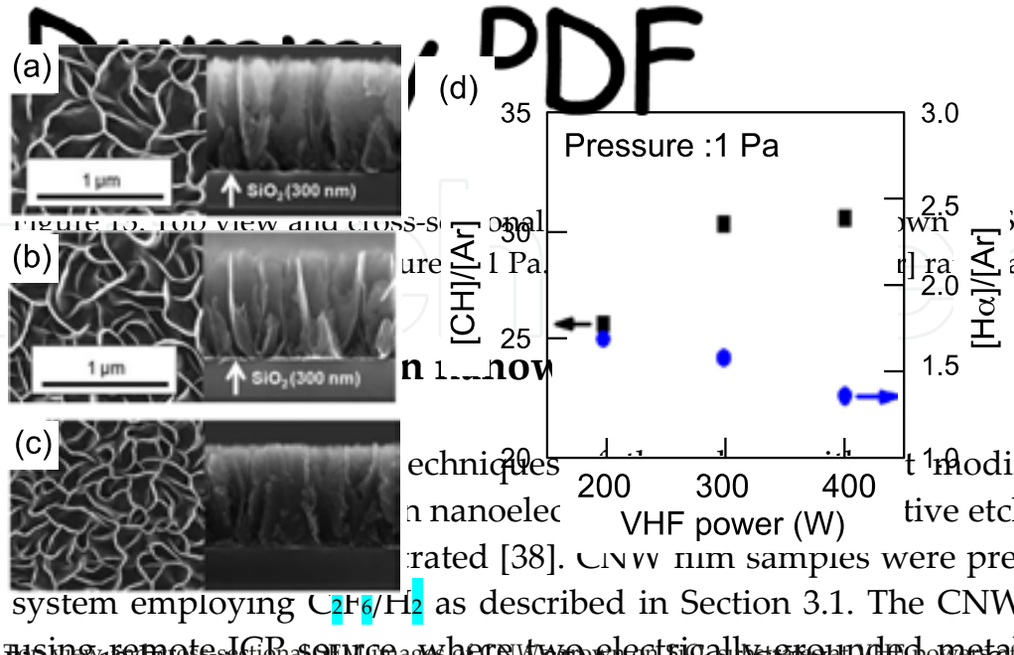

Figure 13. Top view and cross-sectional SEM images of CNWs grown on SiO_2 substrates at VHF power of (a) 200 W, (b) 300 W, and (c) 400 W at constant total pressure of 1 Pa. (d) [CH]/[Ar] and [H]/[Ar] ratios as a function of VHF power [31].

system employing C_2F_6/H_2 as described in Section 3.1. The CNW film sample was e

using remote ICP source, where two electrically grounded metal meshes were insta

ICP.

3.3. Etching of carbon nanowalls

Figures 14(a) and 14(b) show SEM images of CNW films before and after atomic oxyg

of the atomic oxygen etching at 700°C for 5 min, the height of CNW film was reduced

change of wall thickness. In contrast, CNWs were not etched in the O_2 atmosphere wit

indicate that atomic oxygen would react with the top edges of CNWs preferably witho

Figure 13. Top view and cross-sectional SEM images of CNWs grown on SiO_2 substrates at VHF powers of (a) 200 W, (b) 300 W, and (c) 400 W at constant total pressure of 1 Pa. (d) [CH]/[Ar] and [H]/[Ar] ratios as a function of VHF power [31].

3.3. Etching of carbon nanowalls

The selective oxidation techniques of the edges without modification of the graphene planes are essential for the fabrication of novel carbon nanoelectronic devices. A selective etching from the top edges of CNWs using remote oxygen plasma has been demonstrated [38]. CNW film samples were prepared on Si substrates for 30 min using the RI-PECVD system employing C_2F_6/H_2 as described in Section 3.1. The CNW film sample was exposed to oxygen atoms provided using remote ICP source, where two electrically grounded metal meshes were installed at the exit in order to remove irradiation of electrons and ions [38]. The CNW sample was placed on the heater stage 20 cm from the exit of the remote ICP.

Figures 14(a) and 14(b) show SEM images of CNW films before and after atomic oxygen etching, respectively. As a result of the atomic oxygen etching at 700°C for 5 min, the height of CNW film was reduced by approximately 160 nm, without change of wall thickness. In contrast, CNWs were not etched in the O_2 atmosphere without plasma at 700°C. These results indicate that atomic oxygen would react with the top edges of CNWs preferably without ion irradiations.

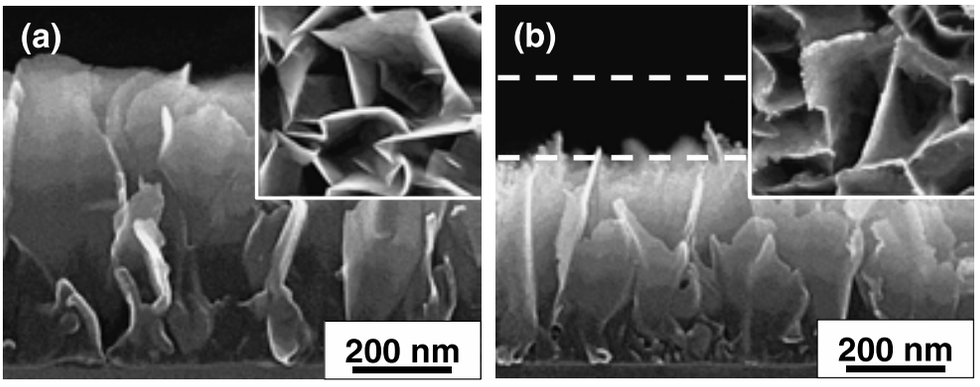

Figure 14. Cross-sectional SEM images of the CNW films (a) before and (b) after atomic oxygen etching at 700°C for 5 min. Insets show views from the top [38].

For comparison, we examined reactive ion etching (RIE) reactions using oxygen plasma. The RIE was carried out for 1 min using dual frequency (60 and 2 MHz) CCP system [38]. Figure 15 shows cross-sectional SEM images of CNW samples (a) before and (b) after oxygen RIE at 20°C for 1 min. As a result of the oxygen RIE, the height of the CNWs decreased drastically, and the top edges of the CNWs were sharpened, and spearlike structures were formed.

Moreover, CNWs were subjected to hydrogen peroxide (H_2O_2) treatment [39]. It has been reported that H_2O_2 treatment can induce oxidative functional groups, such as hydroxyl groups on CNT surfaces, and can selectively oxidize disordered parts on the graphene surface [40]. Accordingly, H_2O_2 treatment has potential for modifying the surfaces of CNWs composed of nanographene domains. CNW film samples were prepared on Si substrates for 45 min using the RI-PECVD system employing C_2F_6/H_2 as described in Section 3.1. The CNW film samples were treated with 30% H_2O_2 solution for 6 and 12 h at 90°C. Then these samples were dried in air at 110°C on a hot plate. Figures 16(a) -16(c) show cross-sectional SEM images of CNWs

http://dx.doi.org/10.5772/61318

decreased drastically, and the top edges of the CNWs were sharpened and spearlike structures were formed.

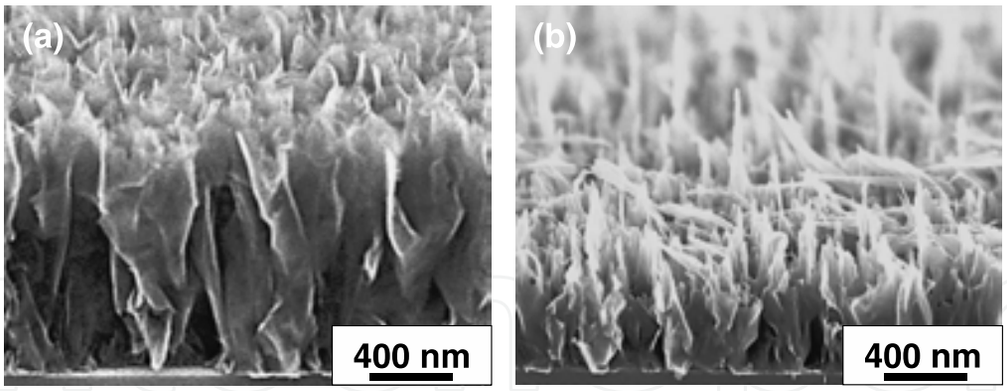

Figure 15. Cross-sectional SEM images of the CNW films (a) before and (b) after oxygen RIE for 1 min [38].

Figure 15. Cross-sectional SEM images of the CNW films (a) before and (b) after oxygen RIE for 1 min [38].

Moreover, CNWs were subjected to hydrogen peroxide (H_2O_2) treatment [39]. It has been reported that H_2O_2 treatment can induce oxidative functional groups, such as hydroxyl groups, on CNT surfaces, and can selectively oxidize disordered parts on the graphene surface [40]. Accordingly, H_2O_2 treatment has potential for modifying the surfaces of CNWs composed of nanographene domains. CNW film samples were prepared on Si substrates for 45 min using the RI-PECVD system employing C_2F_6/H_2 as described in Section 3.1. The CNW film samples were treated with 30% H_2O_2 solution for 6 and 12 h at 90°C. Then these samples were dried in air at 110°C on a hot plate. Figures 16(a)–16(c) show cross-sectional SEM images of CNWs before and after the H_2O_2 treatment for 6 and 12 h. The magnified views of CNW sheets before and after the H_2O_2 treatment were shown in Figures 16(d)–16(f). As a result of H_2O_2 treatment, characteristic nanometer-scale asperities were formed on the wall surfaces of the CNWs as shown in Figures 16(d)–16(f), while the height of CNWs hardly changed. The size of the dents observed in Figures 16(e) and 16(f) was 20–30 nm. The morphology with nanometer-sized asperities on the surfaces of CNWs was stable after the H_2O_2 treatment. This result indicates that the radicals in H_2O_2 solution, such as hydroxyl radicals, react preferentially with the surfaces of CNWs at domain boundaries and induce the characteristic changes in their morphology.

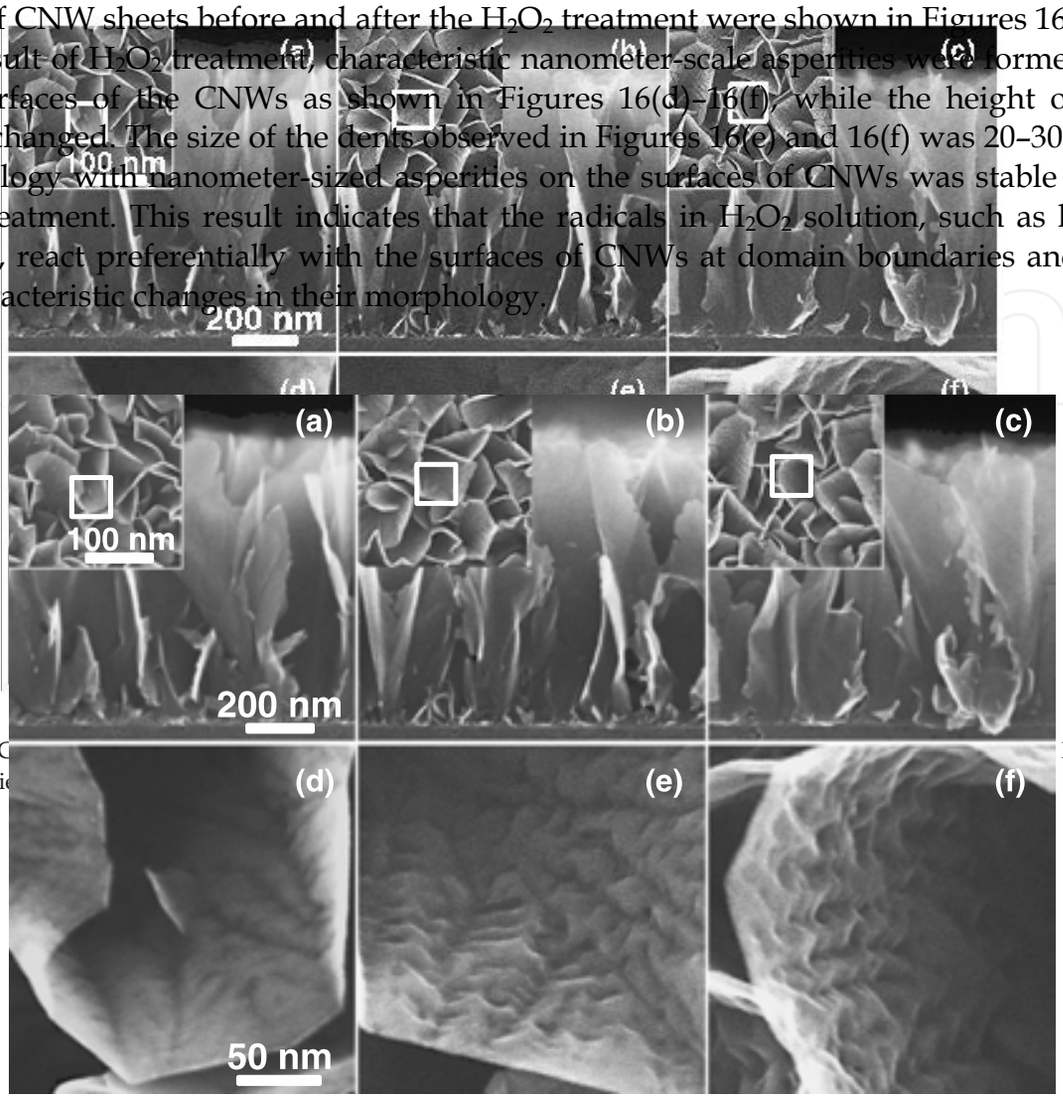

Figure 16. C... Insets show top vi...

In the case of atomic oxygen etching, CNWs are selectively etched from the top edges with almost no change in wall surface morphology, as shown in Figure 14(b). On the other hand, the H_2O_2 treatment induces the characteristic changes in their morphology with keeping the size of CNWs constant. The nanometer-scale asperities on the CNW surface increase the surface area, which would be useful as a platform for supporting metal nanoparticles and organopollutant degradation devices [24,41]. It is noted that such asperities could be reduced by O radical exposure after H_2O_2 treatment, resulting in the reduction of the thickness of CNW sheets. These results, including atomic oxygen etching, oxygen RIE, and H_2O_2 treatment suggest the possibility of realizing etching and thickness control of walls in CNWs, which should be essential for controlling the electrical properties of graphene materials and realizing their applications to electronic devices.

4. Applications of nanoplatform based on vertical nanographene

4.1. Platform for biosensing

Carbon materials have been widely used in both analytical and industrial electrochemistry due to their low cost, wide potential window, relatively inert electrochemistry, and electrocatalytic activity for a variety of redox reactions. Recently, graphene has proved to be an excellent nanomaterial for applications in electrochemistry. Graphene-based materials with large surface area are useful as electrodes for electrochemical sensors and biosensors [42-44]. Electrochemical activity of CNW electrode has been investigated by cyclic voltammetry measurements in an aqueous solution of ferrocyanide and a faster electron transfer between the electrolyte and the nanosheet surface has been demonstrated [21-23]. Dopamine (DA) is a hormone and neurotransmitter that plays a very important role in the human brain and body. Since the changes in the concentration of DA are closely linked to a human's health status, its detection has gained significant attention. Ascorbic acid (AA) and uric acid (UA) are also compounds of great biomedical interest, which all are essential biomolecules in our body fluids. Chemically reduced graphene oxide modified glassy carbon electrode was used to detect these neurotransmitters and biological molecules [42]. In these days, researches on the sensing of biological molecules became popular. Figure 17 shows examples of cyclic voltammogram responses of CNW electrode in the phosphate buffer solution (PBS) with UA, AA, and their mixture at 100 mV/s scan rate. Shang and coworkers demonstrated the excellent electrocatalytic activity of multilayer graphene nanoflakes in simultaneous determination of DA, AA, and UA in PBS [20].

Very recently, electrochemical glutamate biosensor for bioelectronic applications has been demonstrated using platinum (Pt)-functionalized graphene nanoplatelet prepared from graphene oxides [45]. Among the neurotransmitters detected by biosensors, L-glutamate is one of the most important in the mammalian central nervous system, playing a vital role in many physiological processes. The glutamate biosensor is based on the oxidation of glutamate in the presence of glutamate oxidase.

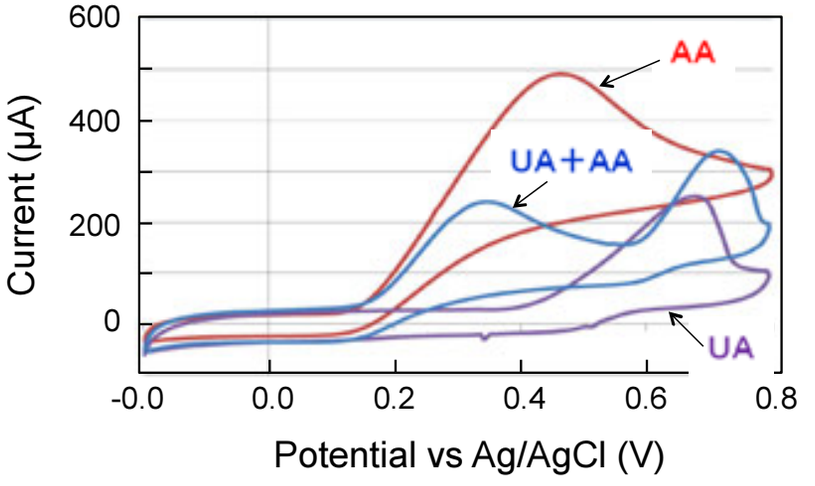

Figure 17. Cyclic voltammogram responses of CNW electrode in PBS with AA, UA, and their mixture at 100 mV/s scan rate.

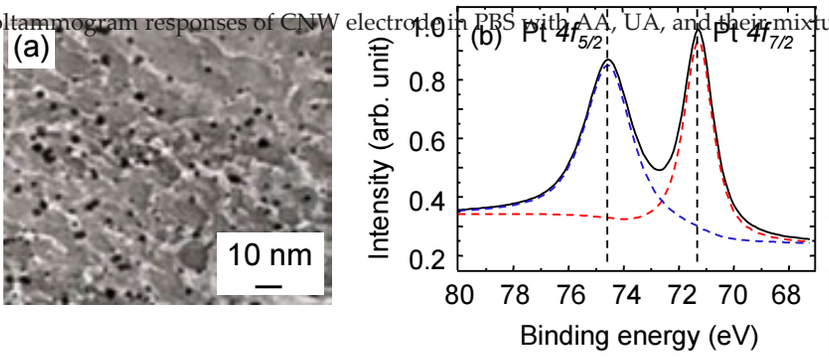

(1)

, although it is
to add various
ussian blue, or
rated in Figure
t itself is com-
particles were
ace of graphite
e electrochem-
n prepared by
alternative ap-
ures, including
hod of deposi-
l-organic com-
sing the metal-
(SCF) [47-49].
in Figure 18(a).
or 30 min. The
ively, and the
pared preferen-

e entire surface
19 shows TEM
30 min and the
methylene blue

contact angles of water lets and the water act angles (WCAs)	the water contact angles (WCAs)
res 20(b)-(e).	Figures 20(b)-20(e).
gures 20(a) and (b),	in Figures 20(a) and 20(b),

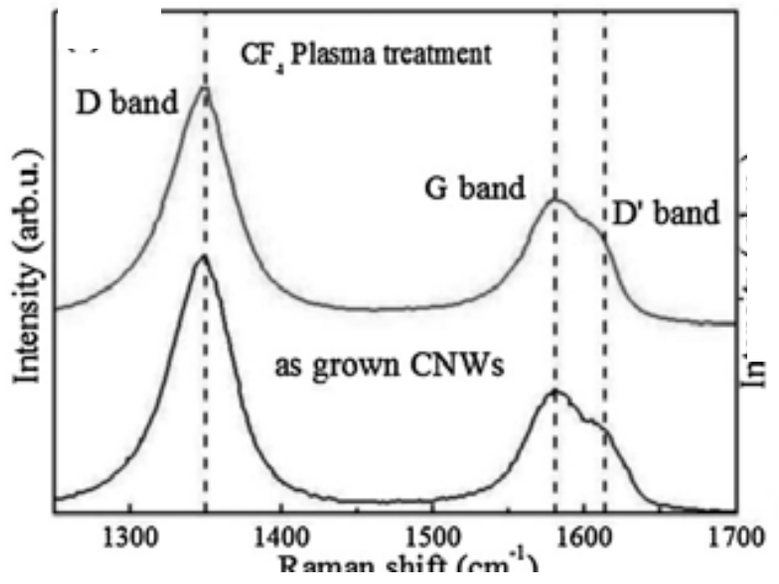

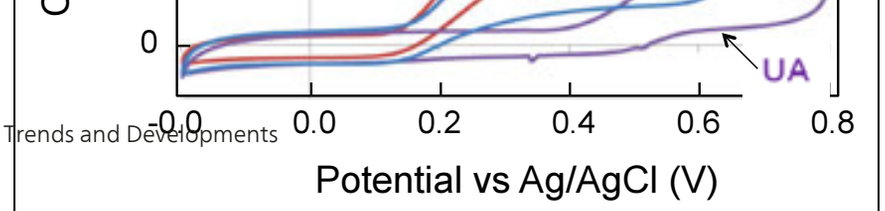

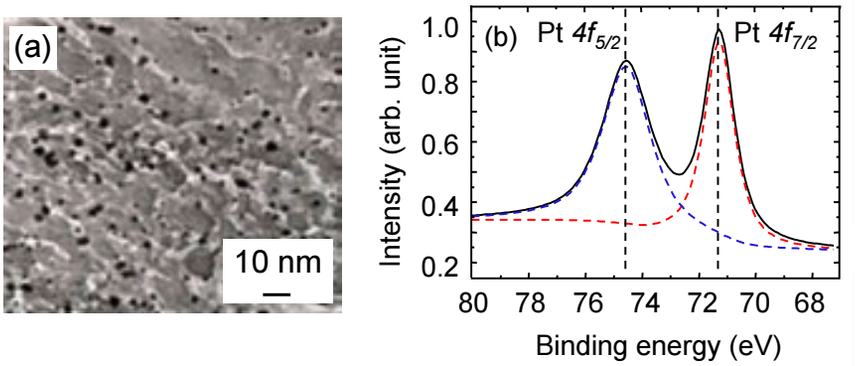

Figure 19. (a) TEM image and (b) XPS profile of Pt nanoparticles after the SCF-MOCFD for 30 min, and (b) XPS profile of the Pt 4f region of the Pt-supported CNW after SCF-MOCFD [50].

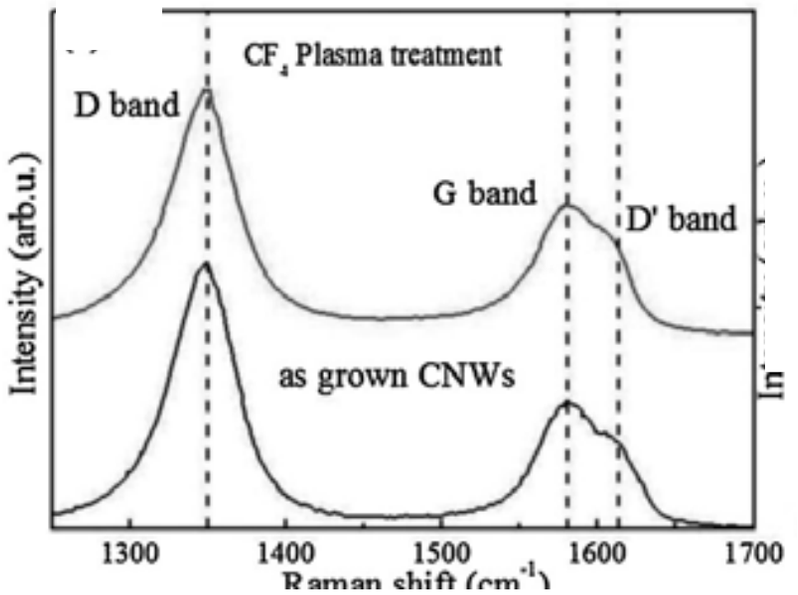

ontact angles of water
ets and the water
ct angles (WCAs)

the water contact angles (WCAs)

es 20(b)-(e).

Figures 20(b)-20(e).

ures 20(a) and (b),

in Figures 20(a) and 20(b),

ne SCF-MOCFD
OCFD [50].

e entire surface
gure 19 shows
or 30 min and
decomposing
sition rate of 6
nform, which
al promise for
lectrochemical
activity offers
lectrochemical
d biosensing.

d (b) the obtained
r 30 min and (b)

trol of surface
ontrol of

surface wettability

In view of the practical applications using CNWs in sensors and platforms for cell culturing, the effects of morphologies of CNWs and their surface properties should be considered systematically. We investigated the surface wettability of CNWs with emphasis on the chemisorption effect by post-processing using plasma treatments [51,52]. Here, CNW

The surface of as-grown CNWs from CH_4/H_2 mixture was terminated with H atoms. After the preparation of CNW film sample using RI-PECVD for 15 min, its surface was oxidized using Ar atmospheric pressure plasma for 1 to 30 s [51,52]. The distance between the CNW film

http://dx.doi.org/10.5772/61318

sample and the atmospheric pressure plasma source was 5 mm. We expect that soft oxidation by oxygen radicals was realized, while the effect of ion bombardment on the surface was negligible during the exposure to atmospheric pressure plasma due to the very short mean free path of ions at the atmospheric pressure. For comparison, the surface of CNW sample was fluorinated for 5 s to add hydrophobic properties to the CNWs. For the fluorination treatment, the CNW sample was exposed to CF_4 plasma generated in the VHF-CCP region of RI-PECVD chamber without using H_2 SWP [51,52].

After the plasma surface treatments using the Ar atmospheric pressure plasma for oxidation and the CF_4 plasma for fluorination in short duration, no noticeable change was observed in the morphology of CNW samples. These results indicate that such short-duration plasma treatments would induce surface chemical functionalization without etching or deposition. Figure 20(a) shows the water contact angles (WCAs) on the CNWs before and after the Ar atmospheric pressure plasma treatment, as a function of plasma treatment duration, together with the WCA after the CF_4 plasma treatment for 5 s. The inset shows SEM image of CNW film sample after Ar atmospheric pressure plasma treatment for 5 s. CNW film samples examined in this experiment have all the same morphology. The side view photographic images of the water droplets on the CNWs before and after the plasma treatments are shown in Figures 20(b)-20(e). The WCAs in the case of diamond films are reported to be approximately 75° on the H-terminated surface and 65° on the O-terminated surface [26]. In contrast, the WCA on the surface of as-grown CNWs prepared employing CH_4/H_2 mixture was 51° [Figure 20(b)]. The surface of as-grown CNWs prepared with CH_4/H_2, of which edges and defects would be partially H-terminated, was rather hydrophilic. After the Ar atmospheric pressure plasma treatment for just 1 s, the WCA was reduced drastically to 11°. Then the WCAs decreased gradually with further increase of the Ar atmospheric pressure plasma treatment duration. As a result of Ar atmospheric pressure plasma treatment for 30 s, the WCA on the CNWs was 5°, indicating that the CNW surface was completely superhydrophilic [Figure 20(d)]. On the other hand, after the CNW sample was exposed to CF_4 plasma for 5 s, the WCA on the CNWs increased significantly to 147°, indicating that the surface of fluorinated CNWs was superhydrophobic [Figure 20(e)]. From these experiments, it was found that the surface wettability of CNW films could be controlled from superhydrophilic to superhydrophobic by the postplasma treatments without changing morphology.

X-ray photoelectron spectroscopy (XPS) measurements were carried out ex situ to analyze the CNW surface exposed to Ar atmospheric pressure plasma for oxidation. Figure 21 shows the composition ratio of O to C (O/C) at the surface of the CNWs as a function of plasma treatment duration. The composition ratio O/C was calculated from the peak intensity ratio of O 1s to C 1s corrected using the relative intensity factors. O content was detected even for the as-grown CNWs without plasma treatment, as shown in Figure 21. Because of ex situ XPS measurements, CNW surface was oxidized when exposed to the atmosphere. Due of the slight existence of oxygen at the surface of CNWs, the as-grown CNWs prepared from CH_4/H_2 would exhibit hydrophilic property as shown in Figures 20(a) and 20(b), in contrast to the hydrophobic surface of H-terminated diamond [53]. As the duration of Ar atmospheric pressure plasma treatment increased, the composition ratio O/C at the surface of CNWs increased rapidly at

indicating that the CNW surface was completely superhydrophilic [Figure 20(d)]. On the other hand, after the CNW sample was exposed to CF_4 plasma for 5 s, the WCA on the CNWs increased significantly to 147˚, indicating that the surface of fluorinated CNWs was superhydrophobic [Figure 20(e)]. From these experiments, it was found that the surface wettability of CNW films could be controlled from superhydrophilic to superhydrophobic by the postplasma treatments without changing morphology

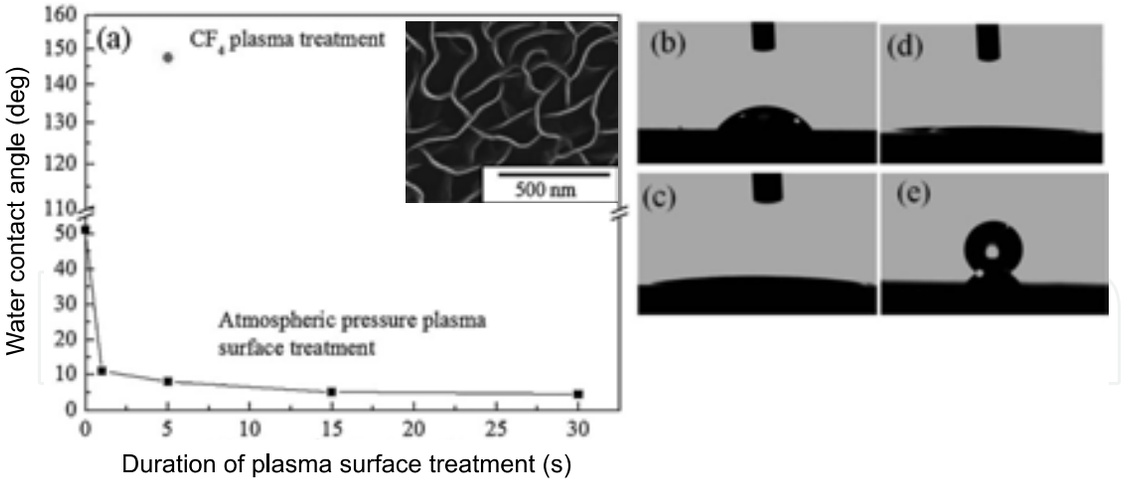

Figure 20. (a) WCAs on CNW films as a function of treatment duration using Ar atmospheric pressure plasma, together with WCA after CF_4 plasma treatment for 5 s. Inset shows SEM image of CNW sample after Ar atmospheric pressure plasma treatment for 5 s. Photos of water droplets on (b) as-grown CNWs, CNWs after Ar atmospheric pressure plasma treatment for (c) 5 s and (d) 30 s, and (e) CNWs after CF_4 plasma treatment for 5 s [52].

first, then very slowly from 5 s, and became almost constant after 15 s. C 1s photoelectron spectra after the plasma treatment were recorded (data not shown). There were various types of oxygen-related components in the CNWs after the Ar atmospheric pressure plasma surface treatment, although components related to the oxidized graphene were small. Therefore, the oxidation occurred only at the edges or surface defects, while the primary structure of CNWs has hardly been changed by the Ar atmospheric pressure plasma exposure.

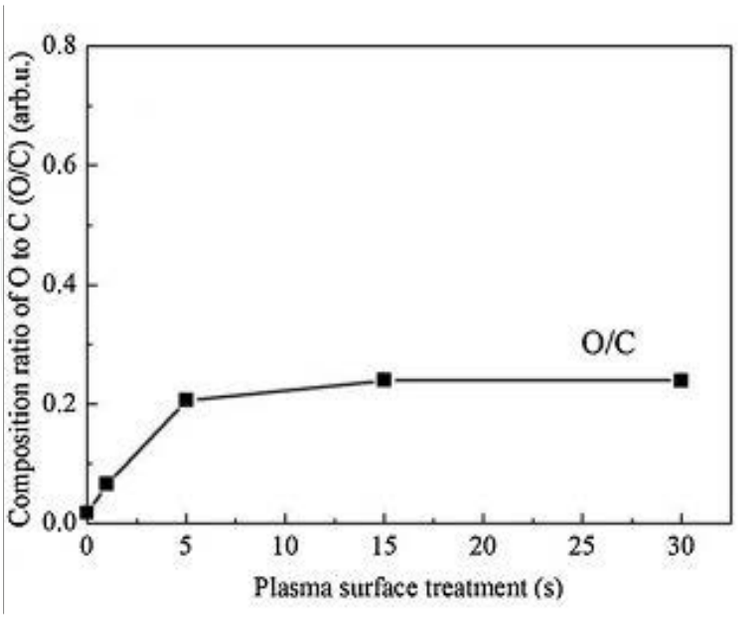

Figure 21. Composition ratio of O to C at the surface of CNWs evaluated from XPS results as a function of plasma treatment duration using the Ar atmospheric pressure plasma [52].

http://dx.doi.org/10.5772/61318

ontact angles (WCAs)	
gures 20(b)-(e).	Figures 20(b)-20(e).
Figures 20(a) and (b),	in Figures 20(a) and 20(b),
	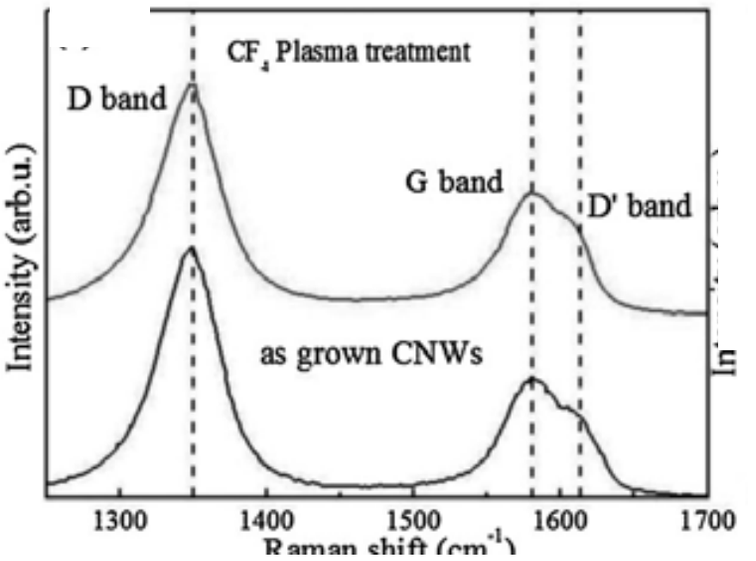

Figure 22. XPS C 1s spectrum of CNWs exposed to CF_4 plasma for 5 s [52].

As mentioned before, by exposure to CF_4 plasma for 5 s, the superhydrophobic surface of CNWs could be easily obtained from the as-grown H-terminated CNWs without changing the morphology of CNWs. The effect of CF_4 plasma treatment for surface fluorination was also investigated using XPS analysis. The composition ratio of F to C at the surface of the CNWs after CF_4 plasma treatment for 5 s was approximately 2.1. The composition ratio F/C was calculated from the ratio of the intensities of F 1s and C 1s peaks, corrected using the relative intensity factors. Figure 22 shows C 1s photoelectron spectrum of CNWs after the surface treatment using the CF_4 plasma for 5 s. The binding energy of 284.6 eV in the XPS spectrum of CNWs is attributed to the C—C (sp^2) bonds. The peaks at 289.1, 291.4, and 293.5 eV in the XPS spectrum shown in Figure 22 are assigned to the CF, CF_2, and CF_3 functional groups, respectively [54]. These three peaks in the XPS spectrum indicate that the F-terminated surface of CNWs was obtained by the CF_4 plasma surface treatment for 5 s, resulting in the realization of superhydrophobic surface.

4.3. Detection of protein using surface-modified carbon nanowalls as electrodes

Surface-oxidized CNW films were used as electrodes to detect bovine serum albumin (BSA) in phosphate-buffered solution (PBS). BSA, a serum albumin protein derived from cows, is often used as a protein concentration standard. CNWs were grown on SiO_2 substrates using RI-PECVD employing C_2F_6/H_2 mixture [5]. For the application of CNWs as an electrode of biosensor, the surface of CNW film was exposed to the Ar atmospheric pressure plasma for obtaining superhydrophilic surface. Electrochemical measurements were conducted using a standard three-electrode setup with an Ag/AgCl reference electrode and a Pt wire counter electrode. The cyclic voltammogram (CV) profiles of as-grown (bare) CNWs (500 nm in height), oxidized CNWs (500 nm), and oxidized CNWs of low height (350 nm) were recorded at scan rate of 100 mVs^{-1}. Figure 23 shows the CV profiles using these CNW electrodes in PBS containing BSA. In the CV profile measured using bare CNW electrode without the Ar

atmospheric pressure plasma treatment, which had slightly hydrophilic surface, weak oxidation and reduction peaks were observed in anode peak potential at 0.2 V and cathodic peak potential at -0.3 V, respectively. In the CV profile using the typical oxidized CNW electrode, on the other hand, a broad oxidation and a high peak reduction currents were observed in anode peak potential of 0.2 V and cathodic peak potential at -0.75 V, respectively. The surface of as-grown CNW electrode could be easily modified into superhydrophilic one by the surface oxidation using the Ar atmospheric pressure plasma. In the case of oxidized CNW electrode with low height, the CV profile exhibited small peak currents due to the small surface area. The results in Figure 23 indicate that superhydrophilic surfaces of CNWs with large surface areas were useful as electrodes for biosensor.

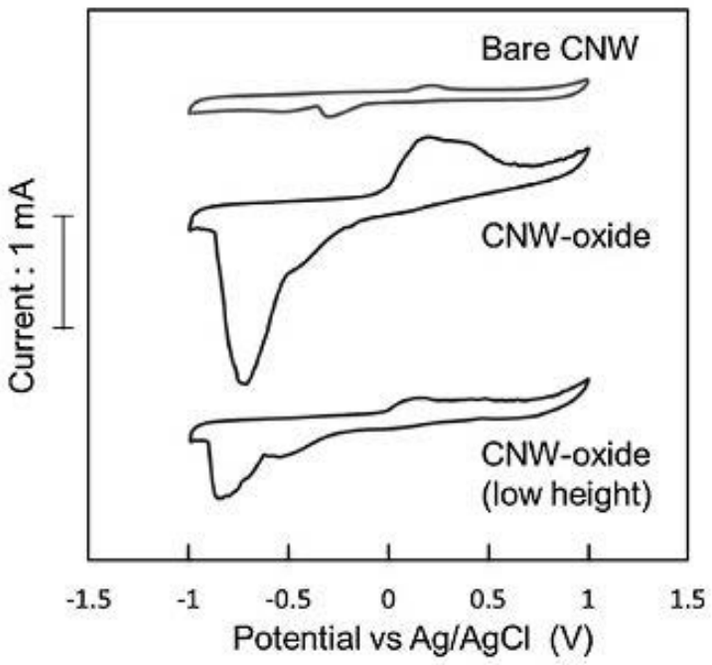

Figure 23. CV profiles of as-grown (bare) CNWs (500 nm in height), oxidized CNWs (500 nm), and oxidized CNWs of low height (350 nm) in PBS containing BSA. Scan rate: 100 mVs^{-1} [52].

4.4. Carbon nanowall scaffold to control culturing of cervical cancer cells

In recent years, cell culturing that uses carbon nanomaterials as scaffolds has been studied intensively [55-57]. The culturing rate is generally discussed with respect to the surface wettability of the scaffold. It has been reported that the cell-culturing rate would peak when the WCA on the scaffold surface is between 60° and 80° [58,59]. Moreover, many factors, including morphology, chemical termination, surface charge, scaffold surface stiffness, and the quantity of adsorbed protein are also essential for determining cell-culturing rates [60-63]. As mentioned in Section 4.2, the wide range control of surface wettability of CNWs was attained by postgrowth plasma treatments [52]. The unique features of CNWs and the variety of surface modification would give CNWs a high potential for scaffold application.

http://dx.doi.org/10.5772/61318

Here, the dependence of cell-culturing rate on the morphology and chemical termination of CNW scaffold was systematically investigated. Three types of CNW scaffolds with different densities (or different wall-to-wall distances) were prepared using RI-PECVD with CH_4/H_2 on quartz plates by changing the total pressure, CCP power, and growth period. The substrate temperature was 560°C. The flow rates of CH_4 and H_2 were fixed at 50 and 100 sccm, respectively. The total pressure was varied in the range of 1 to 5 Pa. The power applied to the SWP was 400 W and that to the CCP was changed in the range of 100 to 500 W. The growth period ranged from 8 to 80 min. Figures 24(a)-(c) show SEM images of the resulting CNW scaffolds with different densities. CNW scaffolds with average wall-to-wall distances of 95, 131, and 313 nm were obtained, which are denoted as "high-density [Figure 24(a)]", "medium-density [Figure 24(b)]", and "low-density [Figure 24(c)]" CNW scaffolds, respectively. The as-grown samples are denoted as H-terminated CNWs.

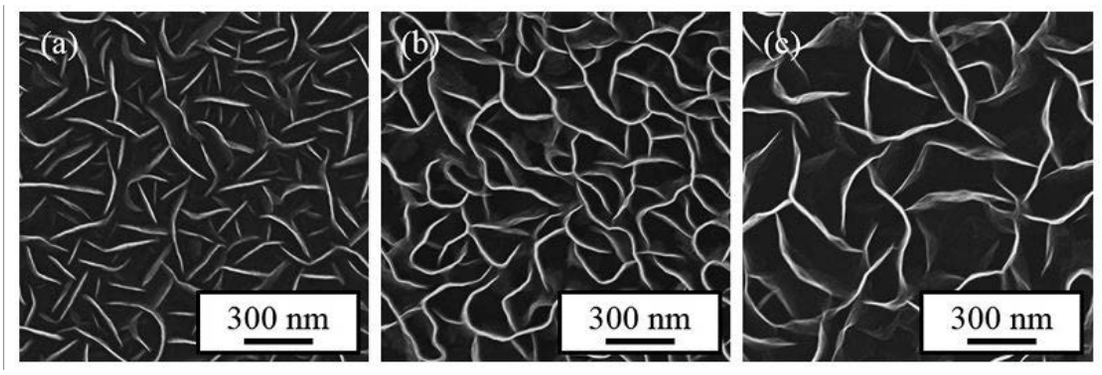

Figure 24. SEM images of (a) high-density CNW, (b) medium-density CNW, and (c) low-density CNW scaffolds prepared using RI-PECVD with CH_4/H_2 [25].

After the preparation of CNWs, some of them were subjected to various plasma treatments to realize the chemical termination of the edges and surfaces of CNWs. For oxygen termination, the CNW film was exposed to the atmospheric pressure plasma employing O_2 (50 sccm)/Ar (2000 sccm) at room temperature for 30 s (O-terminated CNWs). For fluorine termination, the CNW film was set in the VHF CCP employing CF_4 (36 sccm)/Ar (10 sccm) in the RI-PECVD system without SWP at room temperature for 5 s (F-terminated CNWs). The applied CCP power was 200 W, and the pressure was at 107 Pa during the plasma treatment. For nitrogen termination, the CNW film was set in the VHF-CCP region of the RI-PECVD system employing N_2 (12.5 sccm)/H_2 (37.5 sccm) at 560°C for 30 s (N-terminated CNWs). The applied SWP and CCP powers were 400 and 300 W, respectively. The pressure was 1 Pa. Prepared CNW scaffolds with different densities and terminations were put in multiwell cell-culturing plates. Cervical cancer cells (HeLa cells) at a density of 1.0×10^4 cell/cm^2 were seeded on each well. Incubation was conducted under a CO_2 (5%) atmosphere at 37°C for 96 h with 2 ml/well of the medium culture. The cells were maintained in a medium of minimum essential medium (MEM) Eagle, which consisted of 5 ml of L-glutamine (200 mM), 50 ml of fetal bovine serum (FBS), 5 ml of nonessential amino acids for MEM Eagle, and 5 ml of penicillin streptomycin. The HeLa cells cultured on the CNW scaffolds were picked up by using trypsin (0.5 w/v%, 5.3 mmol/l). After

culturing for 24 h, the numbers of the cells with each of two different shapes were counted. One is the nonspreading cell with the circular shape and the other is the spreading cell with the noncircular shape [25].

Figure 25 shows the WCAs on the CNWs after various plasma treatments. The wettability of the CNWs depended on the types of chemical termination, not on the densities of the CNWs. The wettability of CNWs was controllable by plasma treatments in the range from superhydrophilic (WCA ≤ 10°) to near superhydrophobic (WCA ≥ 150°). The insets show the C 1s XPS profiles for the medium-density CNWs with (a) O-termination, (b) N-termination, (c) H-termination (as-grown), and (d) F-termination [52]. As shown in inset (a) of Figure 25, after the Ar/O_2 atmospheric pressure plasma treatment, a small broad peak related to C-O single bonding was observed at around 286.5 eV [64]. The composition ratio O/C was 0.21. After the N_2/H_2 plasma treatment, a broad peak tail was observed at around 285-287 eV, corresponding to nitrogen-related bondings [inset (b)] [65]. The composition ratio N/C was 0.08. In the case of as-grown CNWs, the composition ratio O/C was 0.05. A weak broad peak related to C-O single bonding was observed at around 286.5 eV [inset (c)]. Because of ex situ XPS measurements, CNW surface was oxidized when exposed to the atmosphere. Because of the slight existence of oxygen at the surface of CNWs, the as-grown CNWs exhibited slightly hydrophilic property. In contrast, after the CF_4/Ar plasma treatment, sharp peaks related to $C\text{-}CF_X$ ($X \leq 3$) bonding structures were evident as shown in inset (d). The composition ratio F/C was estimated to be approximately 0.49.

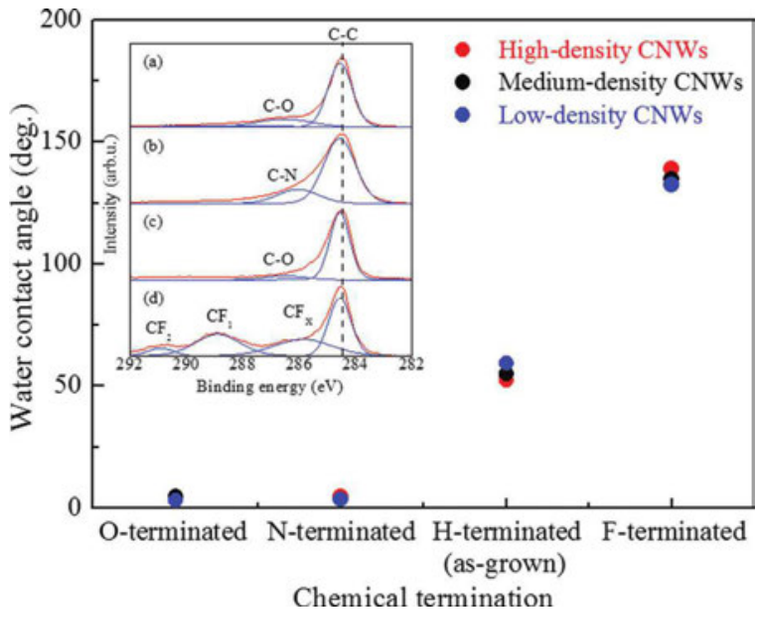

Figure 25. WCAs on the CNWs after various plasma treatments for different terminations. Inset shows C 1s XPS spectra of CNWs, in which the average wall-to-wall distance is 131 nm; (a) O-terminated, (b) N-terminated, (c) H-terminated (as-grown), and (d) F-terminated CNWs [25].

Optical microscope images of HeLa cells cultured on the CNW scaffolds with different terminations and wall densities after incubation for 24 h are shown in Figure 26 [25]. The

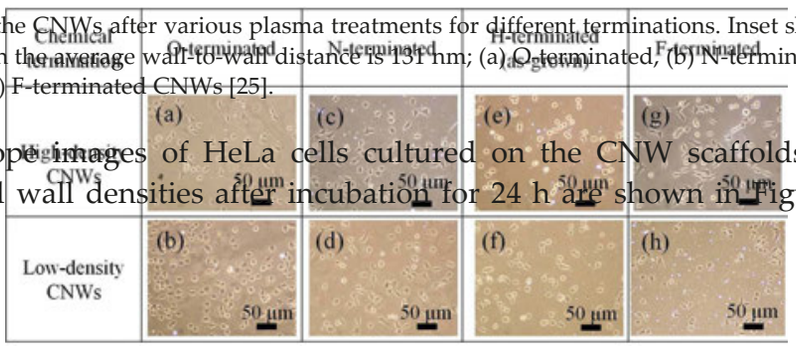

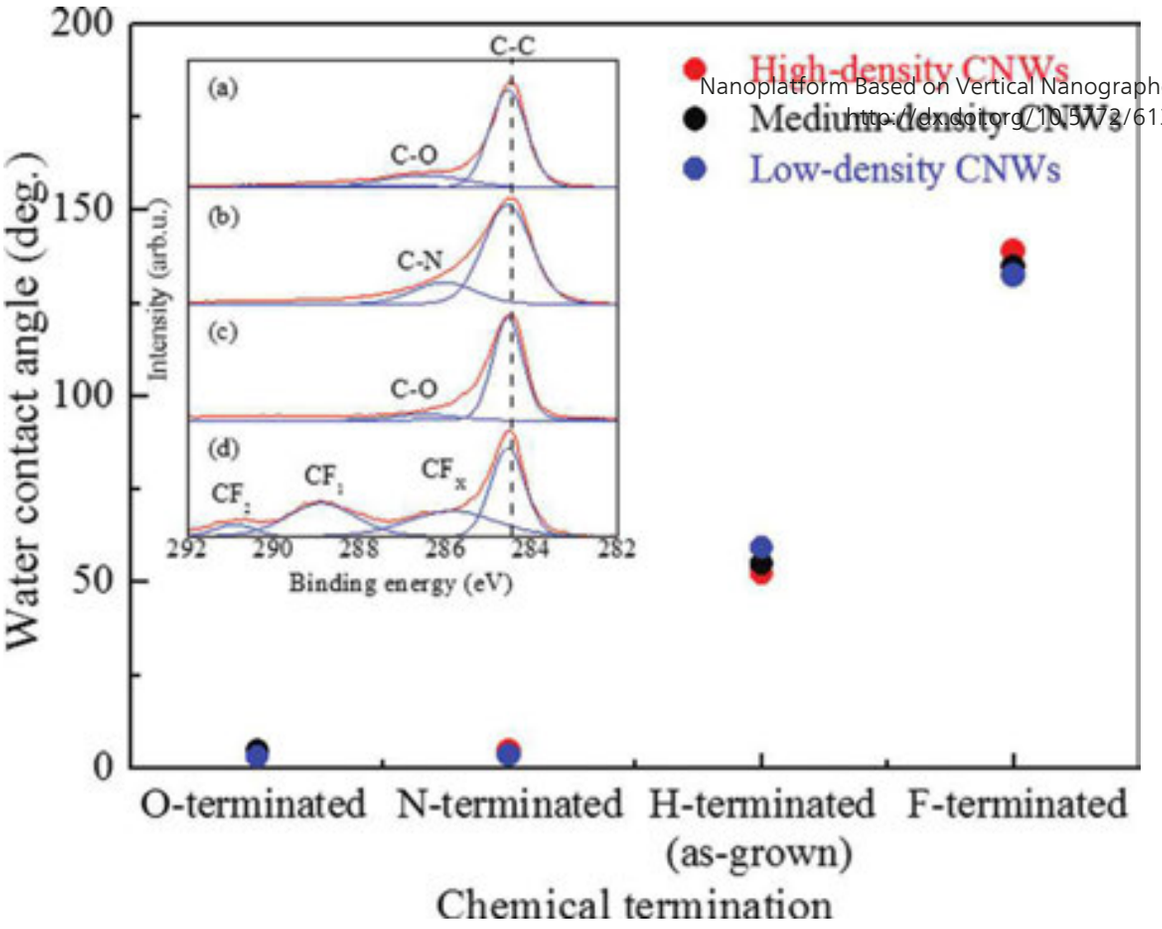

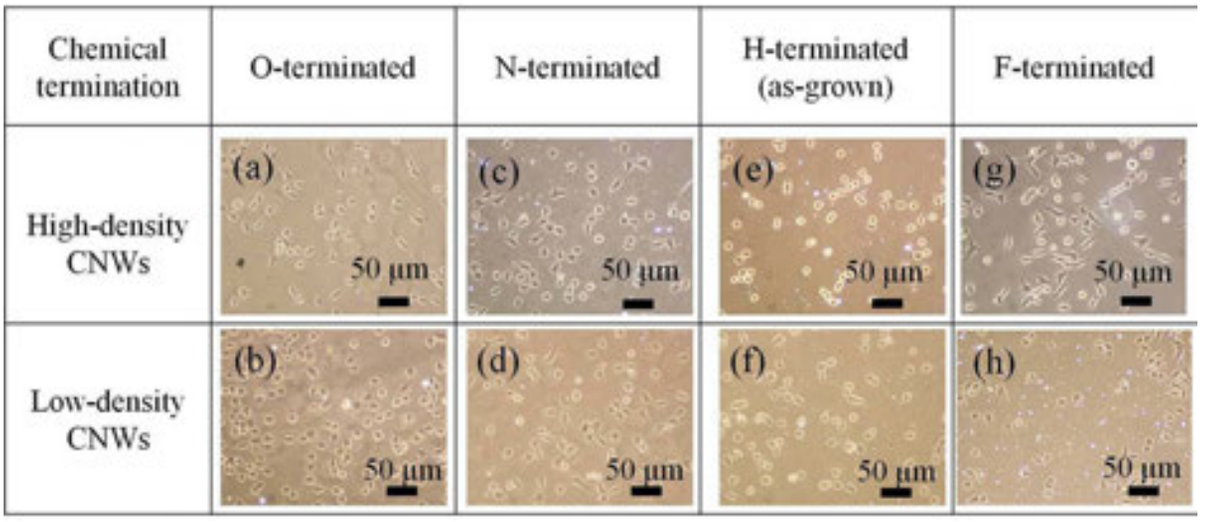

Figure 26. Optical microscope images of HeLa cells cultured on CNW scaffolds with different chemical terminations and wall densities after incubation for 24 h [25].

As a result of systematic investigation on the cell-culturing rates and morphological changes of HeLa cells on CNW scaffolds with respect to the wall densities and wettability of CNWs, it was found that the cell-culturing rates were significantly dependent on the CNW densities but seemed to be independent of the surface wettability of the CNW scaffolds. These results enable us to understand the detailed mechanisms of cell culturing on such scaffolds. Moreover, findings in the present study should also contribute to realize various nano-bioapplications using carbon nanomaterials.

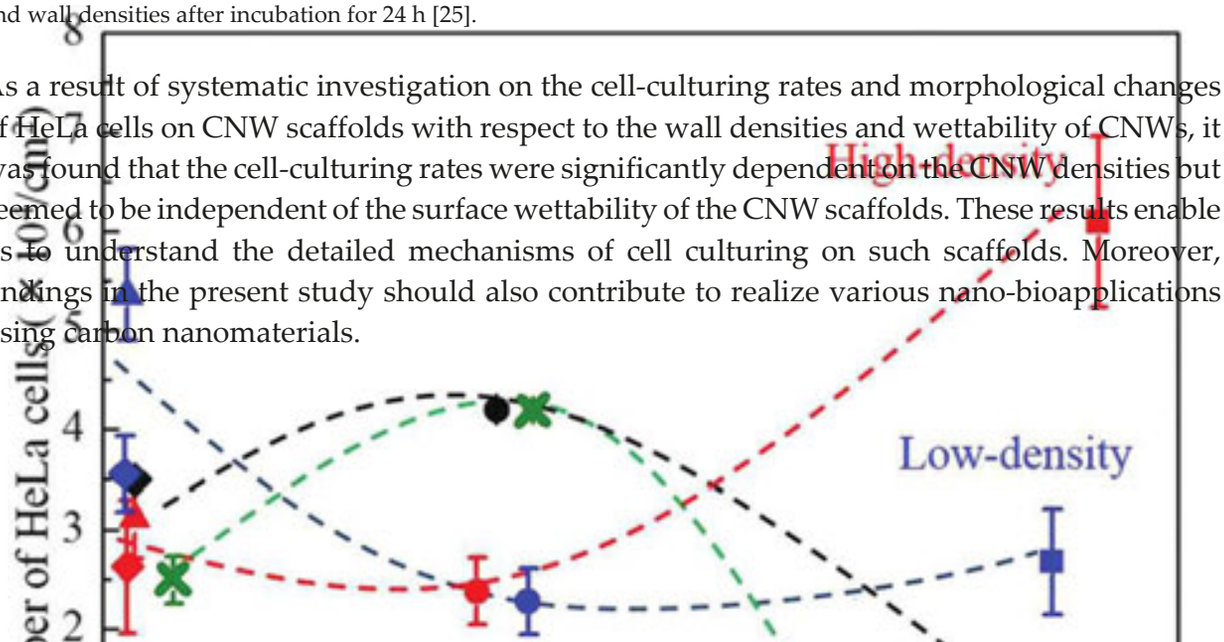

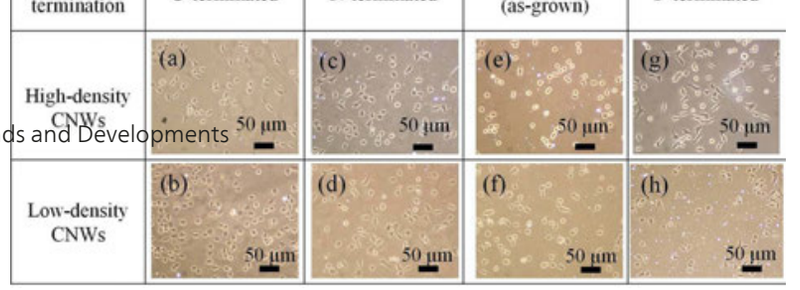

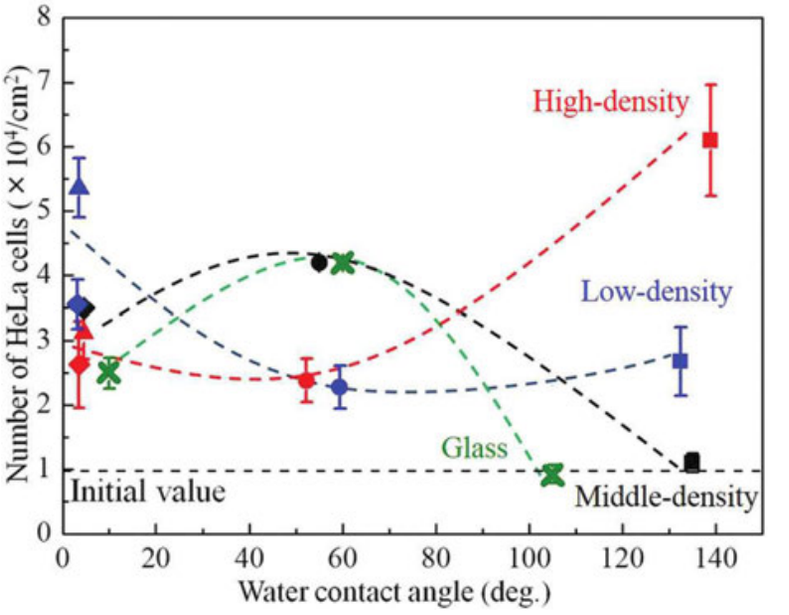

Figure 27. Number of HeLa cells cultured after incubation for 96 h as a function of the water contact angle. For comparison, data for a commercial glass substrate are also presented [25].

5. Conclusion

Carbon nanowalls and related nanocarbon structures composed of nanographene sheets standing vertically on a substrate have been studied intensively. The mazelike architecture of carbon nanowalls with large-surface-area graphene planes and a high density of graphene edges and domain boundaries could prove useful for a number of different applications. Fabrication techniques of carbon nanowalls and possible applications using carbon nanowalls as nanoplatform in the area of electrochemistry and tissue engineering have been described. A radical injection technique was successfully applied to fabricate straight and large-size monolithic carbon nanosheet. The morphology of carbon nanowalls was controlled by changing the total pressure and input power. In addition, the structure of carbon nanowalls was modified by O_2 plasma etching and H_2O_2 treatment.

Using carbon nanowalls as a platform would be the most promising and important application. Carbon nanowalls were used as electrode to detect several biomolecules. In addition, carbon nanowalls were oxidized by the surface treatment using the atmospheric pressure plasma, and proteins such as bovine serum albumin were immobilized on these surface. Moreover, carbon nanowalls were used as scaffold for cell culturing. The dependence of the cell-culturing rates and morphological changes of HeLa cells on carbon nanowall scaffolds with different densities and wettability were systematically investigated.

Nanoplatform based on vertical nanographene offers great promise for providing a new class of nanostructured electrodes for electrochemical sensing, biosensing, and energy conversion applications.

Author details

Mineo Hiramatsu[1*], Hiroki Kondo[2] and Masaru Hori[2]

*Address all correspondence to: mnhrmt@meijo-u.ac.jp

1 Meijo University, Japan

2 Nagoya University, Japan

References

[1] Berger, C.; Song, Z. M.; Li, X. B.; Wu, X. S.; Brown, N.; Naud, C.; Mayo, D.; Li, T. B.; Hass, J.; Marchenkov, A. N.; Conrad, E. H.; First, P. N. & de Heer, W.A. (2006). "Electronic confinement and coherence in patterned epitaxial graphene." *Science*, Vol. 312, No. 5777, pp. 1191-1196, DOI: 10.1126/science.1125925

[2] Yu, Q.; Lian, J.; Siriponglert, S.; Li, H.; Chen, Y. P. & Pei, S. S. (2008). "Graphene segregated on Ni surfaces and transferred to insulators." *Applied Physics Letters*, Vol. 93, Issue 11, 113103 (3 pages), DOI: 10.1063/1.2982585

[3] Li, X.; Cai, W.; An, J.; Kim, S.; Nah, J.; Yang, D.; Piner, R.; Velamakanni, A.; Jung, I.; Tutuc, E.; Banerjee, S.K.; Colombo, L. & Ruoff, R.S. (2009). "Large-area synthesis of high-quality and uniform graphene films on copper foils." *Science*, Vol. 324, No. 5932, pp. 1312-1314, DOI: 10.1126/science.1171245

[4] Wu, Y. H.; Qiao, P. W.; Chong, T. C. & Shen, Z. X. (2002). "Carbon nanowalls grown by microwave plasma enhanced chemical vapor deposition." *Advanced Materials*, Vol. 14, Issue 1, pp. 64-67, DOI: 10.1002/1521-4095(20020104)14:1<64::AID- AD-MA64>3.0.CO;2-G

[5] Hiramatsu, M.; Shiji, K.; Amano, H. & Hori, M. (2004). "Fabrication of vertically aligned carbon nanowalls using capacitively coupled plasma-enhanced chemical vapor deposition assisted by hydrogen radical injection." *Applied Physics Letters*, Vol. 84, Issue 23, 4708 (3 pages), DOI: 10.1063/1.1762702

[6] Wang, J. J.; Zhu, M. Y.; Outlaw, R. A.; Zhao, X.; Manos, D. M.; Holloway, B. C. & Mammana, V. P. (2004). "Free-standing subnanometer graphite sheets." *Applied Physics Letters*, Vol. 85, Issue 7, 1265 (3 pages), DIO: 10.1063/1.1782253

[7] Zhao, X.; Outlaw, R. A.; Wang, J. J.; Zhu, M. Y.; Smith, G. D. & Holloway, B. C. (2006). "Thermal desorption of hydrogen from carbon nanosheets." *Journal of Chemical Physics,* Vol. 124, Issue 19, 194704 (6 pages), DOI: 10.1063/1.2187969

[8] Zhu, M.; Wang, J.; Holloway, B. C.; Outlaw, R. A.; Zhao, X.; Hou, K.; Shutthanandan, V. & Manos, D. M. (2007). "A mechanism for carbon nanosheet formation." *Carbon,* Vol. 45, Issue 11, pp. 2229-2234, DOI: 10.1016/j.carbon.2007.06.017

[9] Hiramatsu, M. & Hori, M. (2006). "Fabrication of carbon nanowalls using novel plasma processing." J*apanese Journal of Applied Physics*, Vol. 45, pp. 5522-5527, DOI: 10.1143/JJAP.45.5522

[10] Kondo, S.; Hori, M.; Yamakawa, K.; Den, S.; Kano, H. & Hiramatsu, M. (2008). "Highly reliable growth process of carbon nanowalls using radical injection plasma-enhanced chemical vapor deposition." *Journal of Vacuum Science & Technology* B, Vol. 26, Issue 4, pp. 1294-1300, DOI: 10.1116/1.2938397

[11] Takeuchi, W.; Ura, M.; Hiramatsu, M.; Tokuda, Y.; Kano, H. & Hori, M. (2008). "Electrical conduction control of carbon nanowalls." *Applied Physics Letters*, Vol. 92, 213103 (3 pages), DOI: 10.1063/1.2936850

[12] Mori, T.; Hiramatsu, M.; Yamakawa, K.; Takeda, K. & Hori, M. (2008). "Fabrication of carbon nanowalls using electron beam excited plasma-enhanced chemical vapor deposition." *Diamond and Related Materials*, Vol. 17, Issues 7-10, pp. 1513-1517, DOI: 10.1016/j.diamond.2008.01.070

[13] Hiramatsu, M.; Nihashi, Y.; Kondo, H. & Hori, M. (2013). "Nucleation control of carbon nanowalls using inductively coupled plasma-enhanced chemical vapor deposition," J*apanese Journal of Applied Physics*, Vol. 45, 01AK05 (6 pages), DOI: 10.7567/JJAP.52.01AK05

[14] Kondo, S.; Kawai, S.; Takeuchi, W.; Yamakawa, K.; Den, S.; Kano, H.; Hiramatsu, M. & Hori, M. (2009). "Initial growth process of carbon nanowalls synthesized by radical injection plasma-enhanced chemical vapor deposition." *Journal of Applied Physics*, Vol. 106, Issue 9, 094302 (6 pages), DIO: 10.1063/1.3253734

[15] Kawai, S.; Kondo, S.; Takeuchi, W.; Kondo, H.; Hiramatsu, M. & Hori, M. (2010). "Optical properties of evolutionary grown layers of carbon nanowalls analyzed by spectroscopic ellipsometry." *Japanese Journal of Applied Physics*, Vol. 49, 060220, DOI: 10.1143/JJAP.49.060220

[16] Seo, D. H.; Kumar, S. & Ostrikov, K. (2011). "Control of morphology and electrical properties of self-organized graphenes in a plasma." *Carbon,* Vol. 49, Issue 13, pp. 4331-4339, DOI: 10.1016/j.carbon.2011.06.004

[17] Krivchenko, V. A.; Dvorkin, V. V.; Dzbanovsky, N. N.; Timofeyev, M. A.; Stepanov, A.S.; Rakhimov, A. T.; Suetin, N. V.; Vilkov, O. Y. & Yashina, L. V. (2012). "Evolution of carbon film structure during its catalyst-free growth in the plasma of direct cur-

rent glow discharge." *Carbon,* Vol. 50, Issue 4, pp. 1477-1487, DOI: 10.1016/j.carbon.2011.11.018

[18] Yang, B.J.; Wu, Y.H.; Zong, B.Y. & Shen, Z.X. (2002). "Electrochemical synthesis and characterization of magnetic nanoparticles on carbon nanowall templates." *Nano Letters*, Vol. 2, No. 7, pp. 751-754, DOI: 10.1021/nl025572r

[19] Giorgi, L.; Makris, T.D.; Giorgi, R.; Lisi, N. & Salernitano, E. (2007). "Electrochemical properties of carbon nanowalls synthesized by HF-CVD." *Sensors and Actuators B: Chemical*, Vol. 126, Issue 1, pp. 144-152, DOI: 10.1016/j.snb.2006.11.018

[20] Shang, N. G.; Papakonstantinou, P.; McMullan, M.; Chu, M.; Stamboulis, A.; Potenza, A.; Dhesi, S. S. & Marchetto, H. (2008). "Catalyst-free efficient growth, orientation and biosensing properties of multilayer graphene nanoflake films with sharp edge planes." *Advanced Functional Materials,* Vo.18, Issue 21, pp. 3506-3514, DOI: 10.1002/adfm.200800951

[21] Luais, E.; Boujtia, M.; Gohier, A.; Tailleur, A.; Casimirius, S.; Djouadi, M.A.; Granier, A. & Tessier, P.Y. (2009). "Carbon nanowalls as material for electrochemical transducers." *Applied Physics Letters*, Vol. 95, Issue 1, 014104 (3 pages), DOI: 10.1063/1.3170033

[22] Tanaike, O.; Kitada, N.; Yoshimura, H.; Hatori, H.; Kojima, K. & Tachibana, M. (2009). "Lithium insertion behavior of carbon nanowalls by dc plasma CVD and its heat-treatment effect." *Solid State Ionics*, Vol. 180, Issues 4-5, pp. 381-385, DOI: 10.1016/j.ssi.2009.01.012

[23] Wang, Z.; Shoji, M. & Ogata, H. (2011). "Carbon nanosheets by microwave plasma enhanced chemical vapor deposition in CH_4-Ar system." *Applied Surface Science,* Vol. 257, Issue 21, pp. 9082-9085, DOI: 10.1016/j.apsusc.2011.05.104

[24] Mase, K.; Kondo, H.; Kondo, S.; Hori, M.; Hiramatsu, M. & Kano, H. (2011). "Formation and mechanism of ultrahigh density platinum nanoparticles on vertically grown graphene sheets by metal-organic chemical supercritical fluid deposition." *Applied Physics Letters,* Vol. 98, Issue 19, 193108 (3 pages), DOI: 10.1063/1.3583672

[25] Watanabe, H.; Kondo, H.; Okamoto, Y.; Hiramatsu, M.; Sekine, M.; Baba, Y. & Hori, M. (2014). "Carbon nanowall scaffold to control culturing of cervical cancer cells." *Applied Physics Letters,* Vol. 105, Issue 24, 244105 (4 pages), DOI: 10.1063/1.4902054

[26] Nemanich, R. J. & Solin, S. A. (1979). "First- and second-order Raman scattering from finite-size crystals of graphite." *Physical Review* B, Vol. 20, Issue 2, pp. 392-401, DOI: 10.1103/PhysRevB.20.392

[27] Kurita, S.; Yoshimura, A.; Kawamoto, H.; Uchida, T.; Kojima, K.; Tachibana, M.; Molina-Morales, P. & Nakai H. (2005). "Raman spectra of carbon nanowalls grown by plasma-enhanced chemical vapor deposition." *Journal of Applied Physics*, Vol. 97, Issue 10, 104320 (5 pages), DOI: 10.1063/1.1900297

[28] Ferrari, A. C.; Meyer, J. C.; Scardaci, V.; Casiraghi, C.; Lazzeri, M.; Mauri, F.; Piscanec, S.; Jiang, D.; Novoselov, K. S.; Roth, S. & Geim, A. K. (2006). "Raman spectrum of graphene and graphene layers." *Physical Review Letters,* Vol. 97, 187401 (4 pages), DOI: 10.1103/PhysRevLett.97.187401

[29] Ferrari, A. C. (2007). "Raman spectroscopy of graphene and graphite: disorder, electron-phonon coupling, doping and nonadiabatic effects." *Solid State Communications,* Vol. 143, Issues 1-2, pp. 47-57, DOI: 10.1016/j.ssc.2007.03.052

[30] Kondo, S.; Kondo, H.; Hiramatsu, M.; Sekine, M. & Hori, M. (2010). "Critical factors for nucleation and vertical growth of two dimensional nano-graphene sheets employing a novel Ar+ beam with hydrogen and fluorocarbon radical injection." *Applied Physics Express,* Vol. 3, 045102 (3 pages), DOI: 10.1143/APEX.3.045102

[31] Cho, H. J.; Kondo, H.; Ishikawa, K.; Sekine, M.; Hiramatsu, M. & Hori, M. (2014). "Density control of carbon nanowalls grown by CH_4/H_2 plasma and their electrical properties." *Carbon*, Vol. 68, pp. 380-388, DOI: 10.1016/j.carbon.2013.11.014

[32] Takeuchi, W.; Takeda, K.; Hiramatsu, M.; Tokuda, Y.; Kano, H.; Kimura, S.; Sakata, O.; Tajiri, H. & Hori, M. (2010). "Monolithic self-sustaining nanographeme sheet grown using plasma-enhanced chemical vapor deposition." *Physica Status Solidi (a),* Vol. 207, Issue 1, pp. 139-143, DOI: 10.1002/pssa.200925230

[33] Naito, S.; Ikeda, M.; Ito, N.; Hattori, S. & Goto, T. (1993). "Effect of rare gas dilution on CH_3 radical density in RF-discharge CH_4 plasma"', *Japanese Journal of Applied Physics*, Vol. 32, Issue 12R, pp. 5721-5725, DOI: 10.1143/JJAP.32.5721

[34] Tachibana, K. (1994). "Detection of H atoms in RF-discharge SiH_4, CH_4 and H_2 plasmas by two-photon absorption laser-induced fluorescence spectroscopy." *Japanese Journal of Applied Physics,* Vol. 33, No. 7B, pp. 4329-4334, DOI: 10.1143/JJAP.33.4329

[35] Takeuchi, W.; Sasaki, H.; Kato, S.; Takashima, S.; Hiramatsu, M. & Hori, M. (2009). "Development of measurement technique for carbon atoms employing vacuum ultraviolet absorption spectroscopy with a microdischarge hollow-cathode lamp and its application to diagnostics of nanographene sheet material formation plasmas." *Journal of Applied Physics*, Vol. 105, 113305 (6 pages), DOI: 10.1063/1.3091279

[36] Hori, M.; Kondo, H. & Hiramatsu, M. (2011). "Radical-controlled plasma processing for nanofabrication." Journal of Physics D: Applied Physics, Vol. 44, 174027 (15 pages), DOI: 10.1088/0022-3727/44/17/174027

[37] Kondo, S.; Kondo, H.; Miyawaki, Y.; Sasaki, H.; Kano, H.; Hiramatsu, M. & Hori, M. (2011). "Reactive ion etching of carbon nanowalls." Japanese Journal of Applied Physics, Vol. 50, 075101 (7 pages), DOI: 10.1143/JJAP.50.075101

[38] Shimoeda, H.; Kondo, H.; Ishikawa, K.; Hiramatsu, M.; Sekine, M. & Hori, M. (2013). "Atomic oxygen etching from the top edges of carbon nanowalls." Applied Physics Express, Vol. 6, 095201 (4 pages), DOI: 10.7567/APEX.6.095201

[39] Shimoeda, H.; Kondo, H.; Ishikawa, K.; Hiramatsu, M.; Sekine, M. & Hori, M. (2014). "Nanostructure modification to carbon nanowall surface employing hydrogen peroxide solution." Japanese Journal of Applied Physics, Vol. 53, 040305 (4 pages), DOI: 10.7567/JJAP.53.040305

[40] Simon, F.; Kukovecz, A. & and Kuzmany, H. (2003). "Controlled oxidation of single-wall carbon nanotubes: a Raman study," AIP Conference Proceedings Vol. 685, p. 185, DOI: 10.1063/1.1628014

[41] Horibe, T.; Kondo, H.; Ishikawa, K.; Kano, H.; Sekine, M.; Hiramatsu, M. & Hori, M. (2013). "Supercritical fluid deposition of high-density nanoparticles of photocatalytic TiO2 on carbon nanowalls." Applied Physics Express, Vol. 6, 045103 (3 pages), DOI: 10.7567/APEX.6.045103

[42] Zhou, M.; Zhai; Y. & Dong, S. (2009). "Electrochemical sensing and biosensing platform based on chemically reduced graphene oxide." Analytical Chemistry, Vol. 81, Issue 14, pp. 5603-5613, DOI: 10.1021/ac900136z

[43] Pumera, M.; Ambrosi, A.; Bonanni, A.; Chng, E. L. K. & Poh, H. L. (2010). "Graphene for electrochemical sensing and biosensing." Trends in Analytical Chemistry, Vol. 29, Issue 9, pp. 954-965, DOI: 10.1016/j.trac.2010.05.011

[44] Hill, E.W. (2011). "Graphene sensors." IEEE Sensors Journal, Vol. 11, Issue 12, pp. 3161-3170, DOI: 10.1109/JSEN.2011.2167608

[45] Hu, J.; Wisetsuwannaphum, S. & Foord, J. S. (2014). "Glutamate biosensors based on diamond and graphene platforms." Faraday Discussions, Vol. 172, pp. 457-472, DOI: 10.1039/c4fd00032c

[46] Kobayashi, K.; Tanimura, M.; Nakai, H.; Yoshimura, A.; Yoshimura, H.; Kojima, K. & Tachibana, M. (2007). "Nanographite domains in carbon nanowalls." Journal of Applied Physics, Vol. 101, Issue 9, 094306 (4 pages), DOI: 10.1063/1.2728781

[47] Machino, T.; Takeuchi, W.; Kano, H.; Hiramatsu, M. & Hori, M. (2009). "Synthesis of platinum nanoparticles on two-dimensional carbon nanostructures with an ultrahigh aspect ratio employing supercritical fluid chemical vapor deposition process." Applied Physics Express, Vol. 2, 025001 (3 pages), DOI: 10.1143/APEX.2.025001

[48] Hiramatsu, M. & Hori, M. (2010). "Preparation of dispersed platinum nanoparticles on a carbon nanostructured surface using supercritical fluid chemical deposition." Materials, Vol. 3, No. 3, pp. 1559-1572, DOI: 10.3390/ma3031559

[49] Hiramatsu, M.; Machino, T.; Mase, K.; Hori, M. & Kano, H. (2010). "Preparation of platinum nanoparticles on carbon nanostructures using metal-organic chemical fluid deposition employing supercritical carbon dioxide." Journal of Nanoscience and Nanotechnology, Vol. 10, No. 6, pp. 4023-4029, DOI: 10.1166/jnn.2010.1996

[50] Hiramatsu, M.; Mitsuguchi, S.; Horibe, T.; Kondo, H.; Hori, M. & Kano, H. (2013). "Fabrication of carbon nanowalls on carbon fiber paper for fuel cell application," Jap-

anese Journal of Applied Physics, Vol. 45, 01AK03 (5 pages), DOI: 10.7567/JJAP.52.01AK03

[51] Watanabe, H.; Kondo, H.; Sekine, M.; Hiramatsu, M. & Hori, M. (2012). "Control of super hydrophobic and super hydrophilic surfaces of carbon nanowalls using atmospheric pressure plasma treatments." Japanese Journal of Applied Physics, Vol. 51, 01AJ07 (4 pages), DOI: 10.1143/JJAP.51.01AJ07

[52] Watanabe, H.; Kondo, H.; Hiramatsu, M.; Sekine, M.; Kumar, S.; Ostrikov, K. & Hori, M. (2013). "Surface chemical modification of carbon nanowalls for wide-range control of surface wettability." Plasma Processes and Polymers, Vol. 10, pp. 582-592, DOI: 10.1002/ppap.201200141

[53] Kaibara, Y.; Sugata, K.; Tachiki, M.; Umezawa, H. & Kawarada, H. (2003). "Control wettability of the hydrogen-terminated diamond surface and the oxidized diamond surface using an atomic force microscope." Diamond and Related Materials, Vol. 12, Issues 3-7, pp. 560-564, DOI: 10.1016/S0925-9635(02)00373-4

[54] Park, H.; Kwon, K.; Lee, S.; Koak, B.; Nahm, S.; Lee, H.; Cho, K.; Kwon, O. & Kang, Y. (1994). "A study on modified silicon surface after CHF3/C2F6 reactive ion etching." ETRI Journal, Vol. 16, No. 1, pp. 45-57, DOI: 10.4218/etrij.94.0194.0014

[55] Cristina, T.; Marsi, O.; Santos, T. G.; Soares, C. P.; Corat, E. J.; Marciano, F. R. & Lobo, A. O. (2012). "Biomineralization of superhydrophilic vertically aligned carbon nanotubes." Langmuir, Vol. 28, Issue 9, pp. 4413-4424, DOI: 10.1021/la300111k

[56] Zhang, X.; Wang, X.; Q. Lu, Q. & Fu, C. (2008). "Influence of carbon nanotube scaffolds on human cervical carcinoma HeLa cell viability and focal adhesion kinase expression." Carbon, Vol. 46, Issue 3, pp. 453-460, DOI: 10.1016/j.carbon.2007.12.015

[57] Nayak, T. R.; Andersen, H.; Makam, V. S.; Khaw, C.; Bae, S.; Xu, X.; Ee, P. L.; Ahn, J. H.; Hong, B. H.; Pastorin, G. & Özyilmaz, B. (2011). "Graphene for controlled and accelerated osteogenic differentiation of human mesenchymal stem cells." ACS Nano, Vol. 5, Issue 6, pp. 4670-4678, DOI: 10.1021/nn200500h

[58] Grinnell, F.; Milam, M. & Srere, P. A. (1973). "Attachment of normal and transformed hamster kidney cells to substrata varying in chemical composition." Biochemical Medicine, Vol. 7, Issue 1, pp. 87-90, DOI: 10.1016/0006-2944(73)90102-6

[59] Maroudas, N. G. (1973). "Chemical and mechanical requirements for fibroblast adhesion." Nature, Vol. 244, Issue 1, pp. 353-354, DOI: 10.1038/244353a0

[60] Brammer, K. S.; Choi, C.; Frandes, C. J.; Oh, S. & Jin, S. (2011). "Hydrophobic nanopillars initiate mesenchymal stem cell aggregation and osteo-differentiation." Acta Biomaterialia, Vol. 7, Issue 2, pp. 683-690, DOI: 10.1016/j.actbio.2010.09.022

[61] Lee, J. H.; Lee, J. W.; Khangt, G. & Lee, H. B. (1997). "Interaction of cells on chargeable functional group gradient surfaces." Biomaterials, Vol. 18, Issue 4, pp. 351-358, DOI: 10.1016/S0142-9612(96)00128-7

[62] Engler, A. J.; Sen, S.; Sweeney, H. L. & Discher, D. E. (2006). "Matrix elasticity directs stem cell lineage specification." Cell, Vol. 126, Issue 4, pp. 677-689, DOI: 10.1016/j.cell.2006.06.044

[63] Ozeki E. & Matsuda, T. (1990). "Development of an artificial extracellular matrix. Solution castable polymers with cell recognizable peptidyl side chain." ASAIO Transactions, Vol. 36, Issue 3, pp.M294-M296

[64] Arima, Y. & Iwata, H. (2007). "Effect of wettability and surface functional groups on protein adsorption and cell adhesion using well-defined mixed self-assembled monolayersiamond surface and the oxidized diamond surface using an atomic force microscope." Biomaterials, Vol. 28, Issue 20, pp. 3074-3082, DOI: 10.1016/j.biomaterials.2007.03.013

[65] Ramanathan, T.; Fisher, F. T.; Ruoff, R. S. & Brinson, L. C. (2005). "Amino- functionalized carbon nanotubes for binding to polymers and biological systems." Chemistry of Materials, Vol. 17, pp. 1290-1295, DOI: 10.1021/cm048357f

[66] Luo, D.; Zhang, G.; Liu, J. & Sun, X. (2011). "Evaluation criteria for reduced graphene oxide." Journal of Physical Chemistry C, Vol. 115, Issue 23, pp. 11327-11335, DOI: 10.1021/jp110001y

IntechOpen